Progress in Aerospace Sciences 86 (2016) 1–19

Contents lists available at ScienceDirect

Progress in Aerospace Sciences

journal homepage: www.elsevier.com/locate/paerosci

Solar sail technology—A state of the art review

Bo Fu*, Evan Sperber, Fidelis Eke

University of California, Davis, One Shields Avenue, Davis, CA 95616, United States

ARTICLE INFO

Article history:
Received 26 February 2016
Received in revised form
5 July 2016
Accepted 6 July 2016
Available online 3 August 2016

Keywords:
Solar sail
Solar radiation pressure
Attitude dynamics
Design and deployment

ABSTRACT

In this paper, the current state of the art of solar sail technology is reviewed. Solar sail research is quite broad and multi-disciplinary; this paper focuses mainly on areas such as solar sail dynamics, attitude control, design and deployment, and mission and trajectory analysis. Special attention is given to solar radiation pressure force modeling and attitude dynamics. Some basics of solar sailing which would be very useful for a new investigator in the area are also presented. Technological difficulties and current challenges in solar sail system design are identified, and possible ideas for future research in the field are also discussed.

Contents

* Corresponding author.
E-mail address: bofu@ucdavis.edu (B. Fu).

http://dx.doi.org/10.1016/j.paerosci.2016.07.001
0376-0421/

1. Introduction

The notion that solar radiation carries with it some form of pressure dates back to Johannes Kepler, who observed that the sun may be causing comet tails to point away from it. In 1610 he wrote in a correspondence with Galileo: "…provide ships or sails adapted to the heavenly breezes, and there will be some who will brave that void." [1]. In the 1860s, James Clerk Maxwell's theory of electromagnetism would yield that electromagnetic fields not only carry energy, but momentum as well. The transferred momentum conveys an effective force, and so radiation pressure is the average force per unit area of all incident and reflected radiation. Early pioneers of solar sailing include Konstantin Tsiolkovsky [2] and Friedrich Tsander [3], who realized that it is possible to attain cosmic velocities using the pressure of solar radiation. Early attempts to construct a functional sailcraft that uses solar radiation exclusively for its propulsion began at the Jet Propulsion Laboratory (JPL) in the seventies. At the time, the development of a solar sail Halley Rendezvous mission was on-going at JPL, and significant effort was expended in designing a practical solar sail for this mission. Although the mission was later dropped by NASA, the lessons learned from this effort laid a solid foundation for solar sailing technology. Much of the work done then is documented by Wright [4]; later work on solar sailing, which focuses on sail trajectory and mission design, is very well summarized by McInnes [5].

Solar radiation pressure (SRP) has been used as a secondary propulsion system in interplanetary space with Mariner 10 and the Messenger spacecraft [6,7]. In this paper, a solar sail (or sailcraft) is considered to be a spacecraft that is propelled mainly or exclusively by solar radiation, and not one where SRP only serves as a secondary means of propulsion. Under such a definition, a typical solar sail would utilize thin sheet(s) of reflective membrane material to harness sun's radiation for propulsion purposes.

The world's first interplanetary solar sail spacecraft called "Interplanetary Kite-craft Accelerated by Radiation Of the Sun" (abbreviated "IKAROS"), was launched by Japan Aerospace Exploration Agency (JAXA) in May 2010. IKAROS's mission demonstrated solar sail propulsion in interplanetary space, and is regarded as a milestone in solar sail technology. Following the IKAROS, the solar sail "LightSail A" from The Planetary Society successfully completed an in-orbit deployment test in June 2015. Three international symposia dedicated to solar sailing were held in 2007, 2010 and 2013. A wide range of research topics was covered including sail design, deployment mechanism, mission analysis, trajectory design, sail material, and sail dynamics. Research interest in solar sails continues to grow even today, as the technology gradually matures.

In order to understand what makes solar sails unique compared to other types of spacecraft, one must take a step back and look at the nature of space flight: a momentum exchange process. Through this momentum exchange process, a spacecraft's linear momentum is altered, and this enables the spacecraft to travel towards its destination. There are two ways in general to achieve linear momentum change for a spacecraft. One is by using propellants, where a portion of craft mass—the propellant mass—is sacrificed. Due to conservation of linear momentum, the craft gains momentum equivalent to that of the lost propellant. Both traditional chemical rockets and the more advanced electric propulsion engines use this method. The difference is that in chemical rockets the velocity of the ejected propellant is much smaller (few thousand meters per second) compared to what occurs in electric propulsion engines (over 10,000 meters per second). Therefore compared to chemical rockets, electric propulsion devices have a higher specific impulse.

The second way to change linear momentum of a spacecraft is through spacecraft–environment interaction, even if the craft mass remains unchanged. Although environmental forces are present regardless of the spacecraft type, most of the time they are treated simply as disturbance forces for spacecraft that rely on propellants. This is because these spacecraft lack the means to make use of the space environmental forces, and the forces themselves are orders of magnitude smaller than the thrust force provided by onboard propellant. A spacecraft that can harvest momentum from the surrounding environment may not need onboard fuel or propellant. Examples of spacecraft capable of environmental momentum exchange include solar sails, electric solar wind sails and magnetic sails. Although these concepts all have the word 'sail' in their names, the momentum exchange mechanism is different in each case. Solar sail in general refers to a type of spacecraft whose main source of thrust is solar radiation. Electric solar wind sails and magnetic sails are spacecraft whose thrust comes mainly from reflecting charged solar wind particles using electric or magnetic fields, thus harvesting momentum from particles in the solar wind.

The term 'sail' naturally evokes an analogy of sailing at sea. A sailship at sea exchanges momentum with its environment – wind, seawater, etc., in order to travel. In the space environment however, the situation is more complex. "Sailing" in space occurs amidst gravitational wells around massive bodies like the planets and the sun. In addition to gravity, there are many other different kinds of environmental forces that can act on a spacecraft. For example, Longuski and Todd [8] found that the space environmental forces on the Galileo spacecraft are estimated to be as shown in Table 1 . This table indicates that at various locations between the earth and Jupiter, forces on the Galileo spacecraft due to solar radiation pressure are order(s) of magnitude higher than other space environmental forces such as those from solar wind, meteoroids, Newtonian drag and magnetic field. Obviously, larger environmental forces indicate greater momentum exchange capabilities with the surrounding environment for a constant mass spacecraft. Thus, in the regions of the solar system visited by the

Table 1
Environmental forces on the Galileo spacecraft in Newtons (N).

Source	Near Venus (0.7 au, $10R_V$)	Near Earth (1 au, $10R_E$)	Interplanetary (3 au)	Near Jupiter (5 au, $10R_J$)
Solar radiation	1.7×10^{-4}	9×10^{-5}	1.1×10^{-5}	3.3×10^{-6}
Solar wind	5.9×10^{-8}	3.1×10^{-8}	3.6×10^{-9}	1.1×10^{-9}
Meteoroids	1.6×10^{-10}	1.1×10^{-10}	9.4×10^{-9}	4.2×10^{-9}
Newtonian drag	3.4×10^{-9}	7.9×10^{-11}	5.3×10^{-11}	5.7×10^{-7}
Magnetic field	5.4×10^{-14}	1.9×10^{-13}	2.1×10^{-11}	1.6×10^{-9}

Please cite this article as: B. Fu, et al., Solar sail technology—A state of the art review, Progress in Aerospace Sciences (2016), http://dx.doi.org/10.1016/j.paerosci.2016.07.001

Galileo spacecraft, a solar sail has a higher potential to harvest momentum compared with other propellantless types of space sails. In the interplanetary environment, SRP forces are also more steady and predictable compared to other environmental forces. This reduces thrust uncertainties in solar sails, allowing reliable trajectories to be designed and followed. The thrust capability and reduced thrust uncertainties make solar sails truly unique among the various types of space sails, especially for interplanetary missions.

In the remainder of this paper, the basic physics of solar sailing, as well as recent advancements in solar sailing technology, will be presented. Special focus is given to a number of subfields of solar sailing technology, including SRP force modeling, solar sail attitude dynamics, solar sail missions and trajectory analysis, and solar sail deployment and design. Review of past contributions, including brief historical overviews and advancements made in the past decade has been given special attention, in the hope that these will be of great interest to students and professionals embarking on solar sail research.

2. Fundamentals of solar sailing

2.1. Solar radiation: energy, momentum and pressure force

Einstein reasoned that the mass of an object is in fact a measure of its energy content, and subsequently the extended version of Einstein's mass–energy equivalence equation could be formulated as the familiar result:

$$E^2 = (m_0c^2)^2 + (pc)^2 \tag{1}$$

where E is the total, or relativistic energy, m_0 is an object's rest mass, p is its momentum, and c is the speed of light. It is readily seen through Eq. (1) how solar radiation even with no rest mass, can carry momentum.

As solar photons hit an object, momentum transfer occurs and a pressure is felt by the object. The magnitude of this pressure, the solar radiation pressure (SRP), depends on the rate of the momentum transfer between solar radiation and the object that it encounters. For example, consider a uniform beam of photons that is applied orthogonally to a flat surface of area A as shown in Fig. 1. Since photons have no rest mass, $m_0 = 0$ in Eq. (1). Assuming that all the momentum from the photons transfers to the surface A as they hit the surface, the time derivative of the right-hand side of Eq. (1) is:

$$2\frac{d}{dt}(pc) = 2c\frac{dp}{dt} = 2cf \tag{2}$$

where f is the magnitude of the force that results from the momentum transfer. The time derivative of the left-hand side of Eq. (1) becomes:

$$2\frac{dE}{dt} = 2WA \tag{3}$$

where W is the radiative flux, which is the amount of power radiated through a given area. Equating Eqs. (2) and (3) gives

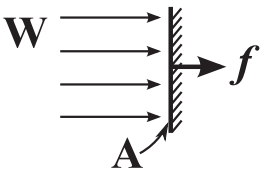

Fig. 1. Radiation pressure force.

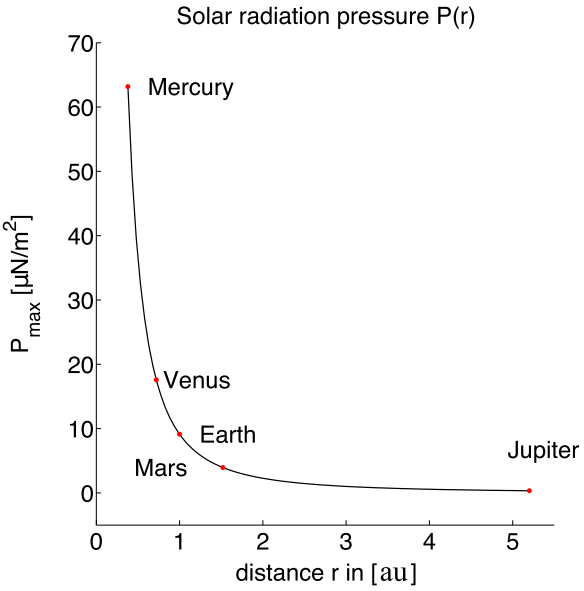

Fig. 2. Maximum SRP for various locations in the solar system.

$$2WA = 2cf \tag{4}$$

and the SRP on surface A is

$$P = \frac{f}{A} = \frac{W}{c} \tag{5}$$

Although momentum of photons can be harvested by a solar sail to provide propulsion, the effectiveness of solar sail propulsion decreases as the sail moves further away from the sun. For a solar sail that is located a great distance from the sun, as will be true for most applications, the sun can be treated as a radiation point source and incident rays of light can be assumed parallel. The solar luminosity of the sun that is its radiative power is $L_\odot = 3.84 \times 10^{26}$ W.[1] The radiative flux, or the amount of solar energy passing through a unit area in one second at a distance r from the sun is:

$$W(r) = \frac{L_\odot}{4\pi r^2} \tag{6}$$

The radiative flux at any distance is typically computed relative to the flux at Earth's mean orbital radius $r_\oplus$ as follows:

$$W(r) = W(r_\oplus)\left(\frac{r_\oplus}{r}\right)^2 \tag{7}$$

The maximum solar radiation pressure $P_{max}(r)$ experienced by an object at a distance r from the sun is determined by $P(r)$ and how the photons are reflected—orientation and reflective properties of the object. Assuming the condition of the object is such that all photons are reflected back to the sun, $P_{max}(r)$ is:

$$P_{max}(r) = 2P(r) = 2W(r)/c = 2W(r_\oplus)\left(\frac{r_\oplus^2}{r^2c}\right) \tag{8}$$

Thus the effective usage range of solar sailing decreases as the sun–sail distance r is increased. Fig. 2 illustrates how the maximum solar radiation pressure P_{max} drops off from Mercury to Jupiter. At earth distance (~1 au) the maximum SRP is about 9 μN/m^2.

[1] Sun facts provided by NASA. See http://solarscience.msfc.nasa.gov.

Please cite this article as: B. Fu, et al., Solar sail technology—A state of the art review, Progress in Aerospace Sciences (2016), http://dx.doi.org/10.1016/j.paerosci.2016.07.001

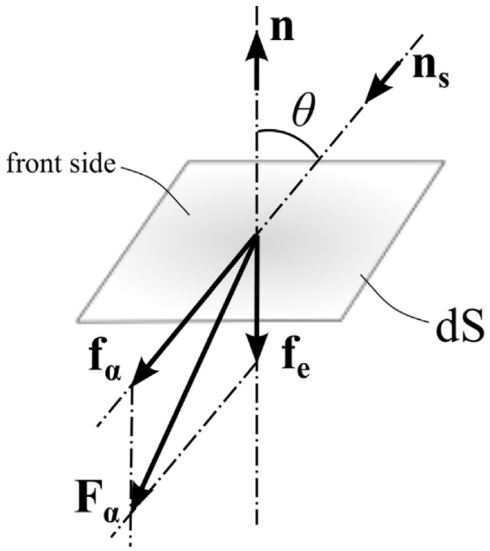

Fig. 3. SRP forces on *dS* for absorption and emission case.

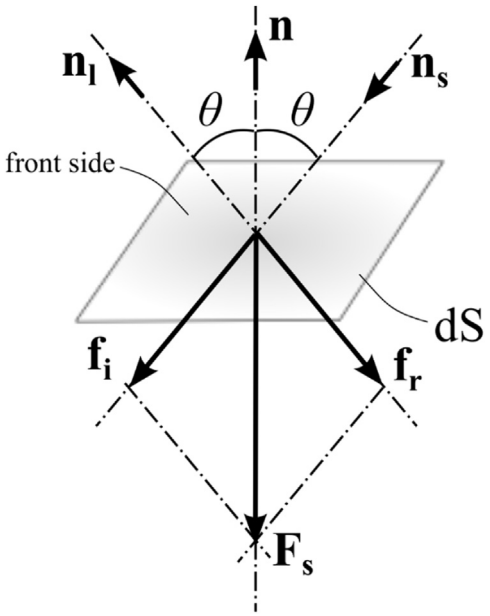

Fig. 4. SRP forces on *dS* for specular reflection case.

2.2. Solar radiation pressure force modeling

2.2.1. Overview

From an engineering point of view, it is sufficient to have a mathematical model that describes how forces and torques are exerted on the sail material as a result of this photon–sail interaction. Note that this interaction can be surprisingly complex. Many factors, such as sail geometry, sail material optical properties, sail temperature, radiation source distance and illuminated area can affect the force and torque on a sailcraft. Hence, developing an appropriate mathematical model for the task at hand is not trivial. Before a discussion of the existing models, a review of pertinent facts about photon–sail interaction is presented. Further details on sail optics can be found in Koblik et al. [9], Forward [10] and McInnes [5].

2.2.2. Photon–sail interaction

When a solar photon strikes a solar sail, it can be assumed that it must be either transmitted, absorbed or reflected. Suppose the probability for these events is τ, α, and ρ, respectively. Then, the following constraint holds:

$$\tau + \alpha + \rho = 1 \tag{9}$$

Consider a differential element $d\mathbf{S}$ of sail material as shown in Fig. 3. Let the incident solar radiation direction $\mathbf{n}_s$ make an angle θ with the surface normal unit vector $\mathbf{n}$. The influence of each force channel on $d\mathbf{S}$ can be treated separately and the total force becomes a weighted sum of each force term.

$$\mathbf{F}_{tot} = \tau\mathbf{F}_\tau + \alpha\mathbf{F}_\alpha + \rho\mathbf{F}_\rho \tag{10}$$

It is easily seen that transmitted photons do not generate a force on $d\mathbf{S}$ ($\mathbf{F}_\tau = 0$). Absorbed photons generate a force $\mathbf{f}_\alpha$ (see Fig. 3) in the direction of the incident radiation as an immediate result of photon momentum transfer:

$$\mathbf{f}_\alpha = \frac{dp}{dt}\mathbf{n}_s = \frac{1}{c}\cdot\frac{dE}{dt}\mathbf{n}_s = \frac{1}{c}\cdot W\cos\theta dS\mathbf{n}_s \tag{11}$$

where W is solar radiative flux.

Since the amount of emitted radiation is directly related to absorbed radiation, radiation pressure force from emission, $\mathbf{f}_e$ (shown in Fig. 3), is discussed here. Assume that the sail is in thermal equilibrium and that the temperature is uniform on the element $d\mathbf{S}$. The equilibrium temperature T_{eq} can be determined through conservation of energy, where incident power equals emitted power:

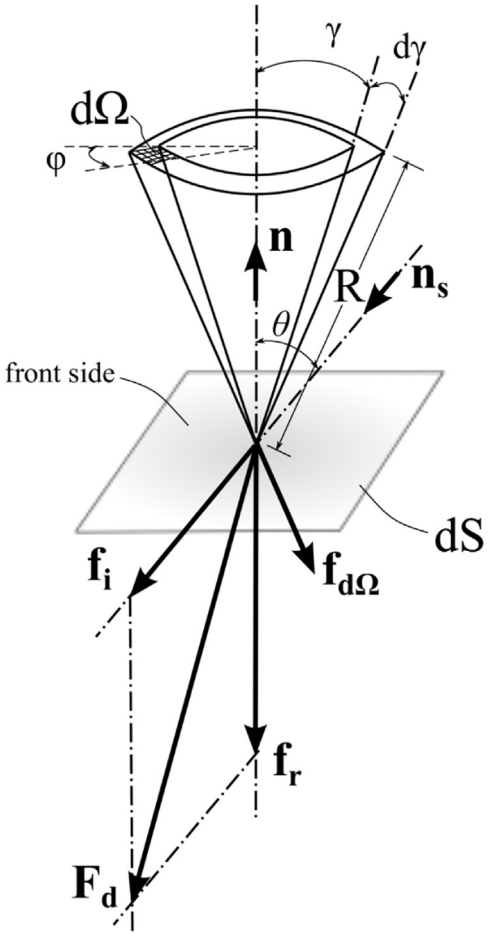

Fig. 5. SRP forces on *dS* for diffuse reflection case.

Please cite this article as: B. Fu, et al., Solar sail technology—A state of the art review, Progress in Aerospace Sciences (2016), http://dx.doi.org/10.1016/j.paerosci.2016.07.001

$$(\epsilon_f + \epsilon_b)\sigma T_{eq}^4 = W\cos\theta T_{eq} = \sqrt[4]{\frac{\alpha W\cos\theta}{\sigma(\epsilon_f + \epsilon_b)}} \tag{12}$$

Hence, ϵ is the surface emissivity, σ is the Stefan–Boltzmann constant and the subscripts 'f' and 'b' indicate front and back sides of the surface, respectively. The resultant force $\mathbf{f}_e$ from emission is thus

$$\mathbf{f}_e = \frac{\sigma T^4}{c}\left(-\varepsilon_f B_f + \varepsilon_b B_b\right)dS\mathbf{n} = \frac{W\cos\theta}{c}\cdot\frac{\varepsilon_b B_b - \varepsilon_f B_f}{\varepsilon_f + \varepsilon_b}dS\mathbf{n} \tag{13}$$

where B is the Lambertian coefficient. Note that if the front and back sides were identical, that is $\epsilon_f = \epsilon_b$ and $B_f = B_b$, the net effect of emission would be null ($\mathbf{f}_e = 0$). From Eqs. (11) and (13), the overall effect of photon absorption and emission is a force $\mathbf{F}_\alpha$

$$\begin{aligned}\mathbf{F}_\alpha &= \frac{1}{c}\cdot W\cos\theta dS\mathbf{n}_s + \frac{W\cos\theta}{c}\cdot\frac{\varepsilon_b B_b - \varepsilon_f B_f}{\varepsilon_f + \varepsilon_b}dS\mathbf{n}\\ &= \frac{W\cos\theta dS}{c}\left(\mathbf{n}_s + \frac{\varepsilon_b B_b - \varepsilon_f B_f}{\varepsilon_f + \varepsilon_b}\mathbf{n}\right)\end{aligned} \tag{14}$$

Generally, reflected radiation can be assumed to be of two types: specularly reflected or diffusely reflected radiation. $\rho\mathbf{F}_\rho$ can thus be expanded to

$$\rho\mathbf{F}_\rho = \rho_s\mathbf{F}_s + \rho_d\mathbf{F}_d \tag{15}$$

where

$$\rho = \rho_s + \rho_d \tag{16}$$

Specular reflection is responsible for the "shininess" of an object. Mirrors and polished metals have high specular coefficients due to lack of surface irregularities. Consider once more a differential element of the sail $d\mathbf{S}$ as shown in Fig. 4. Incident solar radiation whose direction is shown by the unit vector $\mathbf{n}_s$ is reflected in the direction $\mathbf{n}_l$. $\mathbf{n}_l$ lies in the same plane as $\mathbf{n}_s$ and $\mathbf{n}$, and the angle between $\mathbf{n}$ and $\mathbf{n}_l$ is the same as the angle between $\mathbf{n}_s$ and $\mathbf{n}$. Since incident and reflected radiation is symmetric, the surface tangent component of the forces cancel and the net result is a force in a direction normal to the surface. The resultant force from specular reflection is shown by a vector sum of two forces, $\mathbf{f}_i$ and $\mathbf{f}_r$ (see Fig. 4):

$$\mathbf{F}_s = \mathbf{f}_i + \mathbf{f}_r = \frac{1}{c}\cdot W\cos\theta dS\mathbf{n}_s - \frac{1}{c}\cdot W\cos\theta dS\mathbf{n}_l = -\frac{2W}{c}\cdot\cos^2\theta dS\mathbf{n} \tag{17}$$

Diffusely reflected radiation is scattered in all directions. A common model for the diffuse reflection of radiation is Lambert diffusion. A Lambert diffuser scatters incident radiation such that

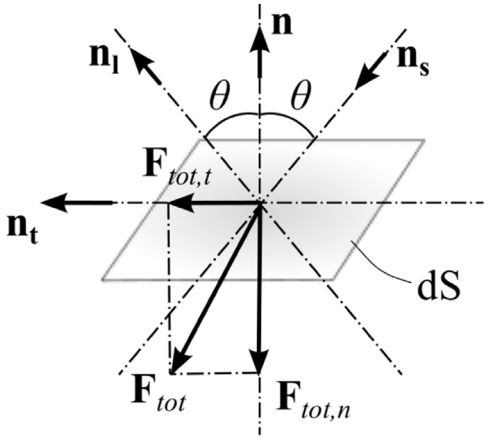

Fig. 6. Components of SRP forces on dS.

the radiant intensity of the reflected radiation when viewed from an angle γ is proportional to the cosine of γ. Since the apparent brightness is the intensity divided by the projected area, which also happens to be proportional to the cosine of γ, the apparent brightness stays constant and does not depend on the observation angle. Similar to the case of specular reflection, the resultant force from Lambert diffusion also consists of two parts (see Fig. 5),

$$\mathbf{F}_d = \mathbf{f}_i + \mathbf{f}_r \tag{18}$$

where

$$\mathbf{f}_i = \frac{1}{c}\cdot W\cos\theta dS\mathbf{n}_s \tag{19}$$

is the force generated by the incident radiation. The force generated by the reflected radiation, $\mathbf{f}_r$, however is different from that of the specular reflection case. It is the sum of forces from all reflected radiation.

Consider a differential area $d\Omega$ shown in Fig. 5. It is formed by first constructing a ring element between two cones on a hemisphere with radius R. The cone angles are γ and $\gamma + d\gamma$, respectively. Then take a differential clock angle ϕ as shown in Fig. 5, the area of the element is thus

$$d\Omega = d\gamma d\varphi\sin\gamma R^2 \tag{20}$$

Since Lambert diffusion is assumed, the radiant intensity at $d\Omega$ is

$$I_\Omega = I_{max}\cos\gamma \tag{21}$$

where I_{max} is the maximum radiant intensity, which can be found using the conservation of radiant flux, as shown below. The total radiant flux is the sum of all radiant intensity over the entire radiated hemisphere:

$$\begin{aligned}\text{total flux} = W\cos\theta dS &= \int I_\Omega d\Omega = \int I_{max}\cos\gamma d\Omega\\ &= \int_0^{\pi/2}\int_0^{2\pi} I_{max}\cos\gamma\sin\gamma R^2 d\varphi d\gamma\\ &= 2\pi R^2 I_{max}\int_0^{\pi/2}\cos\gamma\sin\gamma d\gamma = \pi R^2 I_{max}\end{aligned} \tag{22}$$

Thus

$$I_{max} = \frac{W\cos\theta dS}{\pi R^2} \tag{23}$$

From Eqs. (20) and (23), the radiative flux for the surface $d\Omega$ is

$$W_{d\Omega} = I_\Omega d\Omega = \frac{W\cos\theta dS}{\pi R^2}\cos\gamma d\gamma d\phi\sin\gamma R^2 = \frac{W\cos\theta dS}{\pi}\cos\gamma\sin\gamma\, d\gamma d\phi \tag{24}$$

The resultant force from diffusively reflected radiation through $d\Omega$ is shown by $\mathbf{f}_{d\Omega}$ in Fig. 5. The magnitude $f_{d\Omega}$ is given by

$$f_{d\Omega} = \frac{W_{d\Omega}}{c} = \frac{W\cos\theta dS}{\pi c}\cos\gamma\sin\gamma d\gamma d\varphi \tag{25}$$

Since diffuse reflection is symmetric with respect to the centerline, the tangential component of the resultant force is zero. The only component that is left is a component in the $-\mathbf{n}$ direction, and it is the sum of all forces in the hemisphere:

$$\begin{aligned}\mathbf{f}_r = \iint\cos\left(\gamma\right)f_{d\Omega}\cdot\left(-\mathbf{n}\right) &= \int_{\gamma=0}^{\gamma=\pi/2}\int_{\varphi=0}^{\varphi=2\pi}\frac{W\cos\theta dS}{\pi c}\cos^2\gamma\sin\gamma\\ d\gamma d\varphi\cdot\left(-\mathbf{n}\right) &= \frac{2}{3}\cdot\frac{W\cos\theta dS}{c}\cdot\left(-\mathbf{n}\right)\end{aligned} \tag{26}$$

The factor 2/3 in Eq. (26), as a result of integration, characterizes a Lambertian surface. For non-Lambertian surfaces the specific value of B_f is used in place of 2/3. From Eqs. (18), (19) and (26) the

Please cite this article as: B. Fu, et al., Solar sail technology—A state of the art review, Progress in Aerospace Sciences (2016), http://dx.doi.org/10.1016/j.paerosci.2016.07.001

resultant force from diffuse reflection is

$$\mathbf{F}_d = \frac{W\cos\theta}{c}\cdot(\mathbf{n}_s - \frac{2}{3}\mathbf{n})dS \tag{27}$$

For a non-Lambertian surface Eq. (27) takes the form:

$$\mathbf{F}_d = \frac{W\cos\theta}{c}\cdot(\mathbf{n}_s - B_f\mathbf{n})dS \tag{28}$$

Now it is possible to write an expression of the total force as a result of the photon–sail interaction. From Eqs. (10), (14), (15), (17) and (28), the total force is

$$\mathbf{F}_{tot} = \frac{W}{c}(\alpha\cos\theta\left(\mathbf{n}_s + \frac{\epsilon_b B_b - \epsilon_f B_f}{\epsilon_f + \epsilon_b}\mathbf{n}\right) - 2\rho_s\cos^2\theta\mathbf{n} + \rho_d\cos\theta(\mathbf{n}_s - B_f\mathbf{n}))dS \tag{29}$$

In terms of maximum solar radiation pressure,

$$\mathbf{F}_{tot} = -P(\mathbf{n}_s\cdot\mathbf{n})\left(\alpha\mathbf{n}_s + \alpha\frac{\epsilon_b B_b - \epsilon_f B_f}{\epsilon_f + \epsilon_b}\mathbf{n} + 2\rho_s(\mathbf{n}_s\cdot\mathbf{n})\mathbf{n} + \rho_d(\mathbf{n}_s - B_f\mathbf{n})\right)dS \tag{30}$$

where

$$\tau + \alpha + \rho_s + \rho_d = 1 \tag{31}$$

Notice that the total SRP force has two components, one in the tangential direction and one in the normal direction of $d\mathbf{S}$. Let the tangent direction unit vector be $\mathbf{n}_t$, as shown in Fig. 6. The tangential and normal components of $\mathbf{F}_{tot}$ are:

$$\mathbf{F}_{tot,t} = -\alpha P(\mathbf{n}_s\cdot\mathbf{n})(\mathbf{n}_s\cdot\mathbf{n}_t)dS\cdot\mathbf{n}_t \tag{32}$$

and

$$\mathbf{F}_{tot,n} = -P(\mathbf{n}_s\cdot\mathbf{n})((\alpha + \rho_d + 2\rho_s)\mathbf{n}_s\cdot\mathbf{n} + \alpha\frac{\epsilon_b B_b - \epsilon_f B_f}{\epsilon_f + \epsilon_b} - \rho_d B_f))dS\cdot\mathbf{n} \tag{33}$$

respectively.

In the case of specular reflection only ($\rho_s = 1$), Eq. (30) reduces to:

$$\mathbf{F}_{tot} = -2P(\mathbf{n}_s\cdot\mathbf{n})^2 dS\cdot\mathbf{n} \tag{34}$$

2.2.3. Modeling

In this section existing SRP force models and their underlying assumptions are reviewed. First, it is important to note that in any practical SRP force model, solar radiation is assumed to consist of parallel rays of radiation. This assumption is usually justified because of the relative size and position of the radiation source—the sun, and the radiated object—the solar sail. The large size difference between the sun and the solar sail, together with the fact that a sailcraft can only operate at distances that are orders of magnitude higher than the radius of the sun ($R_\odot = 0.00464$ au) make this assumption reasonable. Perhaps one day solar sailing technology will evolve to a point where orbits of a distance that is comparable to the radius of the sun are allowed, and then this assumption will have to be revised or at least revisited. For discussions of ways to deal with nonparallel rays, see McInnes [5].

The simplest SRP force model assumes that the solar sail is flat and that solar radiation is specularly reflected. This results in the expression derived above (see Eq. (34)) for solar radiation force. In this SRP force model the direction of the sail's thrust is always

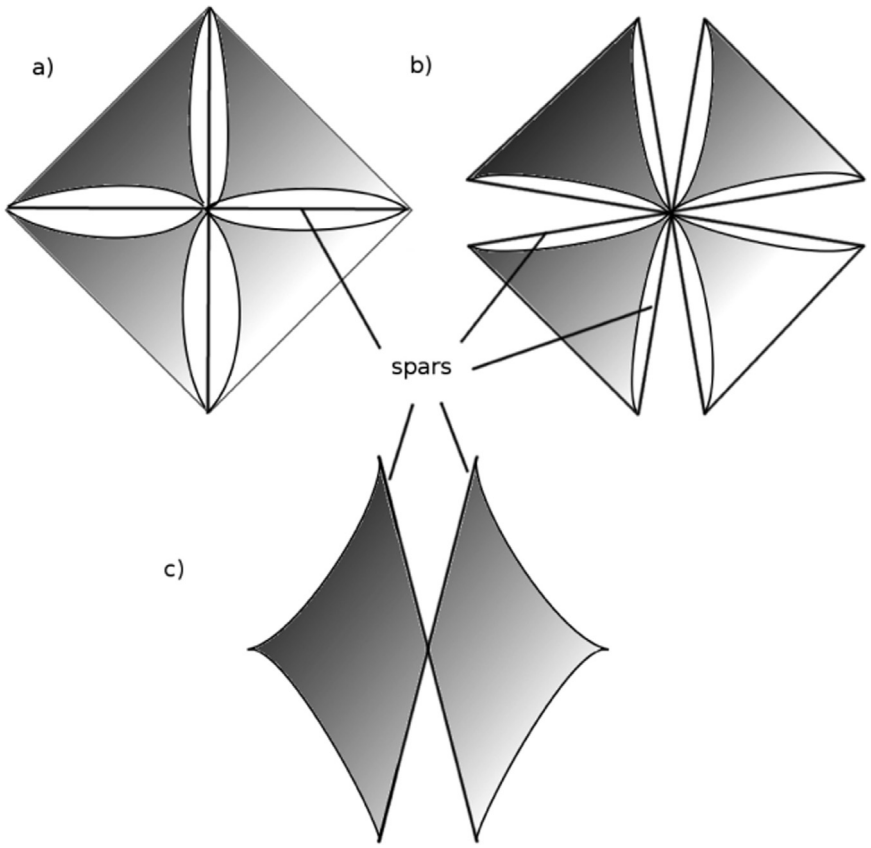

Fig. 7. Rigid sail schemes: clipper (a), quad (b), butterfly (c) [61].

Please cite this article as: B. Fu, et al., Solar sail technology—A state of the art review, Progress in Aerospace Sciences (2016), http://dx.doi.org/10.1016/j.paerosci.2016.07.001

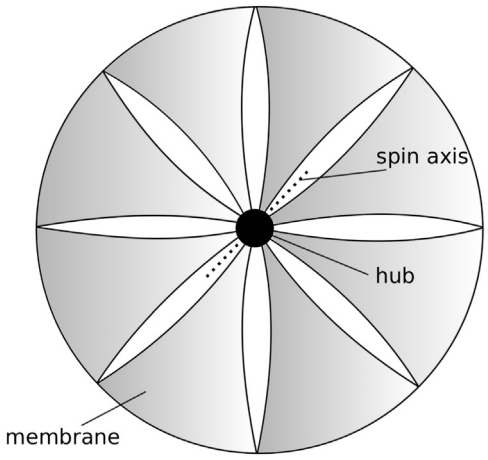

Fig. 8. Disk sail scheme.

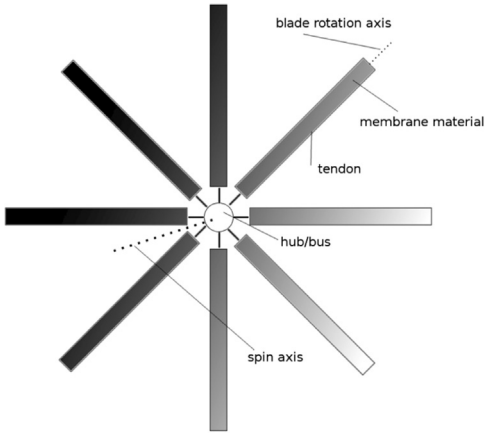

Fig. 9. Heliogyro sailcraft scheme [61].

normal to the sail plane, with magnitude $2\eta\cos^2\theta PA_s$. Here A_s is the sail area and η is an efficiency factor, whose value is between zero and one, that accounts for the loss of thrust due to any other effects. In some studies η is set to 1 for convenience. In most publications, when this SRP force model is used, the sailcraft is referred to as an "ideal solar sail". This force model will be referred to as the ideal solar radiation pressure force model (abbreviated as I-SRP) in this paper. I-SRP is adequate for feasibility studies or preliminary mission analysis for solar sails, and it is widely used even in the most recent publications [11–33].

Another SRP force model that is also widely used includes all the possible photon–sail interactions described in the previous section, and the total force on a flat sail of area A takes the form:

$$\mathbf{F}_{tot} = -PA(\mathbf{n}_s\cdot\mathbf{n})(\alpha\mathbf{n}_s + \alpha\frac{\epsilon_b B_b - \epsilon_f B_f}{\epsilon_f + \epsilon_b}\mathbf{n} + 2\rho_s(\mathbf{n}_s\cdot\mathbf{n})\mathbf{n} + \rho_d(\mathbf{n}_s - B_f\mathbf{n})) \quad (35)$$

This model will be referred to in this paper as optical solar radiation pressure force model (abbreviated as O-SRP) in this paper, since it includes optical parameters of the surface. Although O-SRP can be simplified depending on the choice of parameters, all parameters are assumed to be known constants. O-SRP is used extensively in solar sail research [34–54], as it captures a key characteristic of SRP force that is not present in the I-SRP—there is a component of SRP force, $\mathbf{F}_{tot,t}$ that is parallel to the sail surface:

$$\mathbf{F}_{tot,t} = -\alpha PA(\mathbf{n}_s\cdot\mathbf{n})(\mathbf{n}_s\cdot\mathbf{n}_t)\cdot\mathbf{n}_t \quad (36)$$

For solar sails of arbitrary shape, the total SRP force and moment on the sail can be found by integration. Based on the assumption of invariant surface geometry and total illumination (no part of the sail is shadowed by another object or the sail itself), Rios-Reyes and Scheeres [55,56] showed that starting with O-SRP, expressions for the total sail force and moment can be written compactly in terms of tensors and dyads. This is referred to as the generalized sail model.

There are other SRP force models that are developed based on O-SRP. One of these was developed by Mengali et al. [57], and relaxes the assumption of constant optical parameters, and assumes that they are dependent on sail surface roughness, sun–sail distance r and light incidence angle θ. The dependence on r and θ comes from the fact that sail equilibrium temperature depends on r and θ. The values of parameters used in this model are based on experimental data from the Aurora project (see [58]). Mengali et al. used these data to solve for the equilibrium temperatures (and tabulated them) as functions of r and θ. Since this model uses non-constant optical parameters, it will be referred to as N-SRP.

Another model by Dachwald and Mengali [59] also relaxed the assumption of constant optical parameters, however these parameters are considered to be functions of time only. This allows for the effect of optical degradation, as a result of exposure to high doses of radiation, to be captured. Since this model characterizes optical solar sail degradation, it will be referred to as OD-SRP. The basic idea is that values of certain optical parameters decay exponentially to a final value, and that the amount of this decay is related to the dose of radiation received. Using OD-SRP, McInnes obtained a closed form solution of a solar sail spiral trajectory [60].

There are other factors that influence the prediction of SRP forces. These include sail film wrinkling, surface smoothness, thermal deformation, self-shadowing and billowing. Most of these factors have not been accounted for in SRP force models, mainly because these effects are considered to be secondary for SRP force prediction purposes. For fast traveling solar sails, relativistic effects can influence SRP force predictions. Kezerashvili and Vázquez-Poritz [42] studied first order relativistic effects (in the order of v/c, where v is the sail's orbital speed), known as the Poynting–Robertson effect on solar radiation pressure force modeling. The basic idea is that, in the rest frame of an object moving relative to an isotropic radiation source, radiation will have a component of its incidence vector along the negative spacecraft velocity vector, resulting in a true drag force.

2.3. Solar sail type and categorization

While a multitude of solar sail shapes and sizes have been proposed, the fundamental operating principles remain the same: reflecting surfaces or membranes are used to redirect sunlight for the purpose of creating forces for thrust and torques for attitude control. The shapes of sail membranes and their support structures are commonly used to categorize solar sails. Solar sails that need some kind of supporting structure to maintain their deployment are referred to as rigid sails, while those that do not require a supporting structure to keep the sail deployed are referred to as non-rigid sails.

Rigid sail designs such as the clipper, quad sailer, and butterfly types all maintain sail membrane shape by connecting the membrane edges to rigid structural support spars, though the manner in which the attachment takes place, as well as the number of support spars varies from scheme to scheme (see Fig. 7). For example, the clipper configuration only requires four spars, but may need complex rigging in order to prevent boom deformation due to tension in the membrane. The quad sailer requires two spars per membrane quadrant, thus increasing the mass fraction of structural elements. However, it offers additional control authority

Please cite this article as: B. Fu, et al., Solar sail technology—A state of the art review, Progress in Aerospace Sciences (2016), http://dx.doi.org/10.1016/j.paerosci.2016.07.001

as each quadrant can be rotated independently through motion of the spars in order to generate body torque. The butterfly sailer is a variant that can reduce the weight penalties of structural elements, but may lead to reduced overall thrust due to a decrease in available membrane surface area when compared to designs with more wings or single, contiguous wings. The membrane can be attached at one or multiple points along each spar, depending on individual design specifications. The rigid solar sail variants are the most likely to be chosen for development over other designs in the near term [34]. The additional structure sported by these configurations will help to reduce membrane flexibility, which in most cases will be viewed as a disturbance. These designs also scale well, and are amenable to a broad spectrum of attitude control strategies.

For non-rigid sails, centrifugal forces from sailcraft spin provide the necessary tension in order to keep the sail membranes taught and deployed. Thus non-rigid sails are also referred to as spin sail. In the literature there are two types of solar sails that fall under this category: disk sail and heliogyro. The disk-type solar sail, shown in Fig. 8, consists of a hub, from which a large sheet of sail membrane is deployed. Although referred to as the disk sail, no assumptions are necessarily made regarding the membrane geometry. The IKAROS solar sail, successfully launched in May 2010 by JAXA, is of the disk-type [62]. It consists of a 196 m^2 square membrane that was spin-deployed. The heliogyro was first proposed by MacNeal [63]. The phrase "helio" and "gyro" suggest a relationship with the sun and a spinning nature. A heliogyro solar sail has membranes with large length to width ratios resembling the rotor blades on a helicopter (see Fig. 9). The sail membranes are not part of a contiguous surface, but rather divided into thin strips that are symmetrically arranged about a central hub. Each blade can be rotated about its longitudinal axis as the entire craft spins about a central axis. The blades are weighted at their tips and attached to tendons which help to distribute the centrifugal forces along a blade. The rotation of the entire system spin deploys each blade much like the spin-deployment mechanism of disk sails. One major difference is that the membrane blades of the heliogyro are usually unreeled instead of unfolded when they deploy. Strategically rotating each blade about its longitudinal axis will generate a body torque that the sailcraft can use for attitude control. In this regard, the heliogyro is similar to the quad sail, in which the simple rotation of a sail quadrant produces body torque. The heliogyro was the solar sail configuration selected for one of the earlier sailcraft mission proposals, that of JPL's Halley Rendezvous Sailer in the late 1970s. This design had two banks of six blades, with each blade being 15 m wide and 7.34 km long. A major advantage of a heliogyro design is the ease of blade storage and in-orbit deployment. On the other hand, in order to have a comparable performance with other sail designs, each blade must be long. The large blade dimensions means that dynamical effects such as membrane flexing, bending, and twisting may play a more prominent role in the performance of the spacecraft.

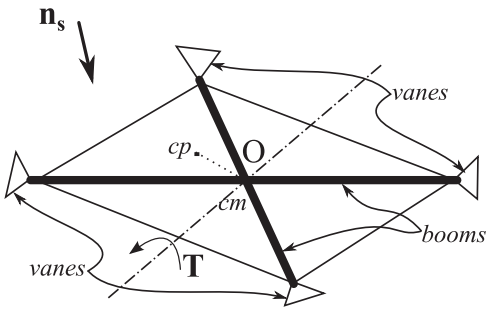

Fig. 10. Control vane method schematics.

As described by Funase et al. [64], a spin-deployed sailcraft offers numerous advantages over sailcraft with membranes deployed using rigid structures. The spacecraft as a whole will have favorable mass to membrane surface area ratio, and as such will be able to generate large accelerations. Additionally, the spinning membrane will have a small amount of angular momentum that will offer a degree of attitude stabilization, as attitude disturbances will result in a precession of the spacecraft spin axis. Another key advantage of non-rigid sail is that their spin allows any performance degradation of sail membrane to be "averaged" over the spin period. For example, damage to the membrane that would otherwise degrade its optical properties and reduce its performance can be mitigated by having it spun. Deployment of non-rigid sails is also relatively simple. However, the membranes of non-rigid sailcraft are ultimately more flexible than those rigidly deployed, and this often has a deleterious effect on attitude control. The large angular momentum of the spinning reflector will also require additional control effort for reorientation. With that said, it is difficult to overstate the impact that deployment difficulty has on the technology readiness level of solar sails, and so this is a major factor in favor of non-rigid sails.

2.4. Solar sail performance matrix

The performance of a solar sail can be expressed using various metrics (see McInnes [5]). The most commonly seen in the literature is the *characteristic acceleration* a_0, which by definition is the acceleration imparted by solar radiation on a solar sail when the sail is orthogonal to the sun at a distance $r=1$ au from the sun,

$$a_0 \triangleq \frac{\eta P_0 A}{m} \tag{37}$$

where

$$P_0 \triangleq P_{max}(r=1) \tag{38}$$

is the maximum SRP at 1 au from the sun and m and A are, respectively, the mass and area of the solar sail. η is a dimensionless constant with a value between zero and one. It is essentially an efficiency factor used to account for the various factors that can cause the characteristic acceleration to deviate from its ideal value ($\eta=1$). In the remainder of this paper, η is taken to be equal to 1 for simplicity.

The magnitude of the gravity force F_g felt by a solar sail is

$$F_g = G\frac{mM}{r^2} \tag{39}$$

where G is the gravitational constant, and M and m are the masses of the sun and sail, respectively. Recall from Eq. (8) that F_g changes with an inverse distance squared relationship similar to that of

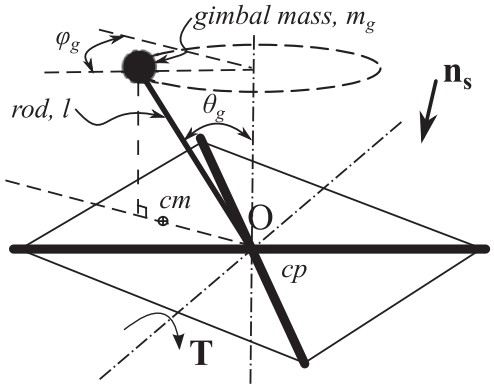

Fig. 11. Gimbal mass method schematics.

Please cite this article as: B. Fu, et al., Solar sail technology—A state of the art review, Progress in Aerospace Sciences (2016), http://dx.doi.org/10.1016/j.paerosci.2016.07.001

$P_{max}(r)$. Because of this the solar sail *lightness number*, β, which is a dimensionless value defined as the ratio between solar radiation acceleration and solar gravitational acceleration, does not change for a solar sail operating at different regions in space.

$$\beta \triangleq \frac{P_{max}A}{GmM/r^2} = 2W\left(r_\oplus\right)\left(\frac{r_\oplus^2}{r^2 c}\right)A\cdot\frac{r^2}{GmM} = 2W\left(r_\oplus\right)\left(\frac{r_\oplus^2}{GmMc}\right)A = constant \tag{40}$$

Similar to a_0, β gives a measure of the effectiveness of a solar sail's ability to use SRP, regardless of the size of the sail.

Another performance metric is the *sail loading* σ_s, defined as the ratio of total mass of the sailcraft to the overall sail area. The smaller the sail loading, the more efficient the sail is for carrying payload. For a solar sail with a flat surface area A and mass m, assuming all photons is specularly reflected, sail loading is given by:

$$\sigma_s = \frac{m}{A} \tag{41}$$

There is a relationship between a_0 and σ_s:

$$a_0 = \frac{P_0}{\sigma_s} \tag{42}$$

For a sail that is not flat, obtaining an expression for the characteristic acceleration is no longer straightforward, and an integration method is needed to determine the total force acting on the sail such that a comparison can be made with flat sails.

3. Solar sail attitude dynamics and control

3.1. Overview

For a sailship at sea, the position of its sails is controlled by sailors to ensure that the ship stays on course, even though the environmental forces, such as the wind forces and current forces, are constantly changing. For a solar sail in space, the sailcraft's orientation also needs to be controlled to ensure the sailcraft that follows the desired mission trajectory, as gravity forces and solar radiation pressure forces change. The orientation of a solar sail directly determines its thrust vector, hence attitude control is required to steer the sailcraft. Although there exist many methods for spacecraft attitude control, such as using control moment gyros, reaction wheels and thrusters, these methods may not work well for solar sails. For a solar sail, the center of mass (cm) is usually designed to coincide with the center of pressure (cp) of the sail when fully deployed. However, manufacturing and deployment tolerances and errors will generally create an offset distance between sail cm and cp. This offset will lead to a disturbance attitude torque which needs to be countered by the craft's attitude control system in order for the sailcraft to maintain its attitude.

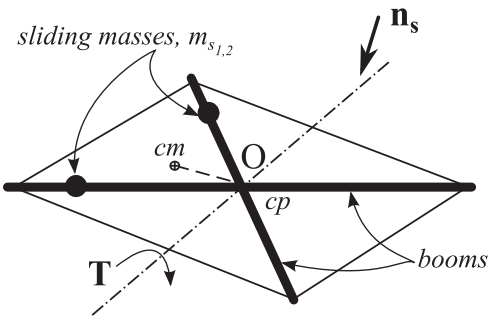

Fig. 12. Sliding method schematics.

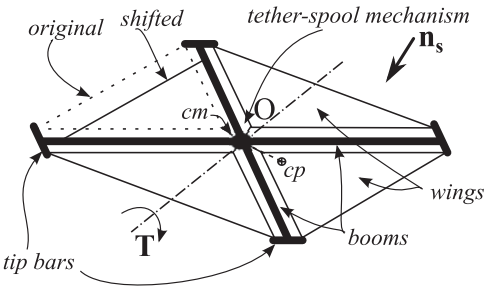

Fig. 13. Shifted wings schematics.

Conventional attitude control methods cannot effectively maintain the sail's attitude for several reasons, as first discussed by Wie [34]. One reason is that the amount of attitude torque needed to counter the solar radiation disturbance torque can be quite large compared to the typical control torque for conventional spacecraft. Wie argued that for a 40×40 m sailcraft, the solar radiation pressure disturbance torque could be 100 times larger than what is typically encountered in a geosynchronous communication satellite [34]. A second reason is that typically a solar sail has a long mission lifetime, and so propellant based attitude control systems would not be suitable. A propellant based attitude control system would also defeat the purpose of using a solar sail in the first place.

Other issues arise when considering conventional attitude control methods for large angle attitude adjustment. For solar sails in general, the mass of the sail components is distributed over a large area, giving the craft a moment of inertia that is relatively large compared to a spacecraft of similar mass. To effectively control the sailcraft attitude, large control moments are needed, limiting the use of conventional attitude control techniques for effective attitude control. The mass of the attitude control system itself is also an important factor in the design of an attitude control system for a solar sail. One parameter to consider when designing an attitude control system for a solar sail is the ratio of the control system to the sailcraft mass, as this provides a way to evaluate the effectiveness of the attitude control system.

Fortunately, it is also possible to take advantage of the fact that under solar radiation pressure, an offset between the sail cm and cp generates attitude torques. By having an attitude control strategy that allows a controlled cm–cp offset, desired attitude torques can be generated. In this way the source of attitude control torque is solar radiation pressure, hence attitude control also becomes propellantless. Many methodologies based on the cm–cp offset idea have been proposed in the literature in the last decade. In the sections that follow, various solar sail attitude control methods that utilize a cm–cp offset for attitude control are discussed.

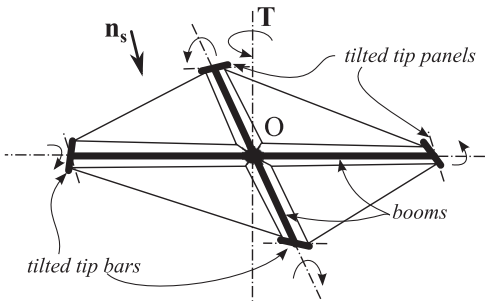

Fig. 14. Tilted wings schematics.

Please cite this article as: B. Fu, et al., Solar sail technology—A state of the art review, Progress in Aerospace Sciences (2016), http://dx.doi.org/10.1016/j.paerosci.2016.07.001

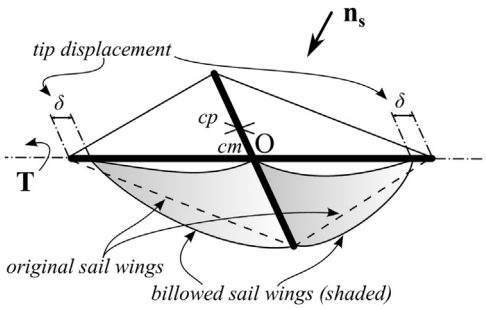

Fig. 15. Billowed wings schematics.

3.2. Attitude control method for rigid sailcraft

3.2.1. Control vane method

Consider a sailcraft with vanes as shown in Fig. 10. The sailcraft is simplified to be a craft that consists of two booms, four triangular pieces of sail membrane which cover the spanned areas of the booms, and four triangular control vanes which are attached to the end tip of the booms. The control vanes are made out of the same reflective material as the sail, and each has two rotational degrees of freedom. Thus, the attitude control system has a total of eight degrees of freedom. Although the vanes are chosen to be triangular shaped in this paper, it can be of any shape in general. Fig. 10 is not drawn to scale, as the control vanes are enlarged for illustration purposes. Initially, the sailcraft cm and cp are designed to be at the center *O*. By rotating the control vanes, the sail cp moves and no longer overlaps with sail cm. This allows a body torque to be generated, which can then be used for attitude control of the sailcraft.

It is difficult to trace the origin of this idea in the literature. Fig. 10 illustrates the application of the idea of control vanes to a square solar sail. However, it can be applied to different types of rigid sails. Even in the case of a square sail, four vanes are not required for attitude control. However, a degree of control redundancy is welcomed in spacecraft design. Documentation on control vanes (and other) methods for solar sail attitude control dates back to 1992, in Wright's book, *Space Sailing* [4]. Wie [35] studied control vanes, and derived the equations of motion for a solar sail with control vanes. In his study the normal direction of each control vane surface is constrained to be in a plane formed by the sail normal vector and the sail boom. This constraint on vane direction simplifies the number of control inputs from eight to four. Using the control vane method, a body torque which consists of three components is generated as a result of eight control inputs. It is easier to compute the body torques from a known state of the sail, which include the current orientation of the sail and the vanes. However due to nonlinearities in the sail model, computing a set of control vane angles based on desired body torque values, is somewhat challenging. This under-constrained control allocation problem has been studied by Choi and Damaren [65], and algorithms were developed to address this issue. The possibilities of self-shadowing which hinders effective body torque generation were studied by Kun [11], in which boundaries of control vane motion that prevents self-shadowing are discussed and a control allocation scheme is developed. Other issues regarding control vanes, such as deployment sensitivity, have been studied by Quadrelli and West [66].

3.2.2. Gimbaled masses method

A mass m_g can be attached to a solar sail through a rigid rod l, as shown in the case of a square solar sail in Fig. 11. l has two rotational degrees of freedom, as determined by a cone angle θ_g and a clock angle ϕ_g in Fig. 11. The length of rod l and the size of mass m_g are exaggerated for illustration purposes. In real sails m_g will be much smaller than sail mass m, which results in a very small out-of-plane component of cm. Thus in the following discussions it is assumed that cm lies on the sail plane. When the rod is orthogonal to the sail, sailcraft cm coincides with cp. As the gimbal's position changes, cm also shifts to a new position which lies on the orthogonal projection of the rod l on the sail surface, as shown in Fig. 11. Since there is an offset between sail cm and cp, a body torque results, and can be utilized for attitude control purposes. Many have also considered the use of payload mass as the gimbaled mass, in order to improve mass efficiency of the solar sail. The first mention of gimballed mass control in the literature is by Angrilli and Bortolami [67]. Other work on gimbaled mass attitude control includes a solar sail that is three-axis stabilized by gimbaling the spacecraft on an extended boom [68]. Wie [35] developed a two-dimensional linear model of a solar sail orbiting the Earth equipped with a gimbaled payload used for attitude control. He then demonstrates through the use of a PID controller that both reorientation and attitude stabilization can be performed with the system subject to gravity gradient, pitch period excitation, and thrust vector misalignment torques. For a gimbaled solar sail, spin torque cannot be generated, and only two-axis attitude control torques can be generated at a given time. Therefore a combination of rotations will be needed in order to reorient a solar sail to any given direction. Nonlinear equations of motion of a three-dimensional gimbaled solar sail were presented by Sperber et al. [69], in which algorithms for attitude reorientation and attitude regulation were also developed.

3.2.3. Sliding masses method

Instead of using a gimbaled mass, sliding masses (also known as trim masses or ballast masses) can be used, as shown in Fig. 12. Two masses, m_{s_1} and m_{s_2} are attached on the sail booms as shown. Each mass has one translational degree of freedom—translation along the respective booms. When the masses are at the center of the sail, cm coincides with cp. As the masses translate along the booms, the position of cm changes. An offset between cm and cp thus exists and creates a body torque.

Similar to the gimbaled mass, the ballast masses used can also be payload masses, increasing sail efficiency. As sail cm and cp always lie in the sail plane, no spin body torque can be generated using sliding masses method alone, and a combination with other attitude control methods which can generate a spin is desired. An example of using sliding masses together with other attitude control method that uses vanes was presented by Adeli et al. [70]. Another study by Wie and Murphy [71] showed a solar sail design whose main attitude control system uses the sliding masses method. The system equations of motion were derived by ignoring nonlinear terms associated with the speed of the sliding masses. For controller design purposes, simple actuator dynamics was assumed. Scholz et al. [72] used the simplified sliding masses dynamic model to study the performance of such a solar sail numerically. Many aspects of the system parametric sensitivity were

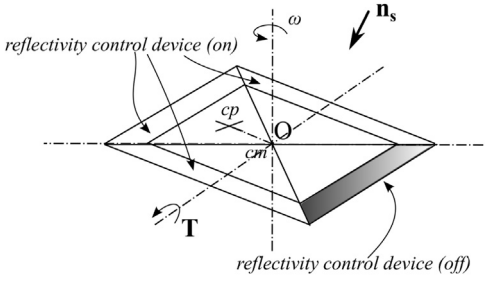

Fig. 16. Reflectivity control device schematics.

Please cite this article as: B. Fu, et al., Solar sail technology—A state of the art review, Progress in Aerospace Sciences (2016), http://dx.doi.org/10.1016/j.paerosci.2016.07.001

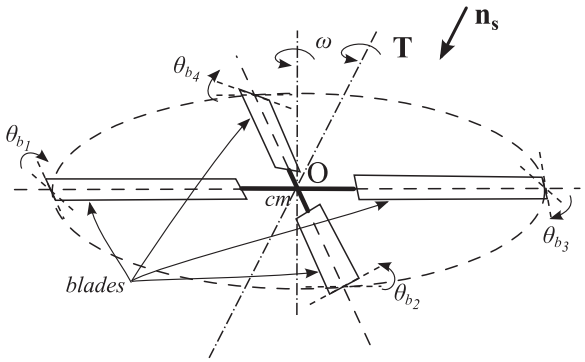

Fig. 17. Heliogyro attitude control schematics.

studied for different attitude maneuvers, and performance of sail of different sail mass and sliding masses was evaluated based on near-optimal maneuver time. The sliding masses approach has great potential for use in future solar sail missions.

3.2.4. Shifted wings method

A square solar sail configuration shown in Fig. 13 is used to demonstrate the shifted wings (or shifted panels) attitude control method. In Fig. 13, the square solar sail differs from what was previously shown by Figs. 10–12. It has tip bars that are attached to the end of each boom. Four pieces of sail membrane, or wings, are connected to the sail at three points by constant force springs: two at the tip bars and one at the center via tethers. The center consists of a tether-spool mechanism that could reel in part of the sail if needed. Originally, all wings are fully displaced as shown. In this position, the cp coincides with cm, and both are located at the center point *O*. For each wing there is one translational degree of freedom. When one wing is reeled in (left-top wing in Fig. 13), the cp of the sail shifts away from *O*. For this attitude control method to work, a significant portion of the sailcraft mass must be located at the center. In this way the cm of the craft after any shift of the wings will remain almost at the center. As a cp–cm offset is now created by shifting the sail wing, attitude control torque is generated. For a sailcraft whose wings make up a large portion of the overall sail mass, the sail cm also shifts with cp, and the shifted wing method becomes less efficient in generating attitude control torque. However, one can still reel in a larger part of the sail wing to generate adequate control torque. Since the reeled wing mass is located at the center hub, cm–cp shift grows rapidly as a larger part of the wing is reeled in.

The method of shifting the sailcraft itself to generate attitude control torque was mentioned by Wright [4] and later developed by Wie [35], who designed and simulated an attitude controller for this case. As all wings are in the same plane whether shifted or not, no spin torque can be generated by simply shifting the sail wings. The tilted wings method, as will be described in the next section, is able to compensate for the lack of spin torque production in shifted wings.

3.2.5. Tilted wings method

Consider a sailcraft with similar layout as the one used to illustrate the shifted wings method, as shown in Fig. 14. In the tilted wing configuration the tip bars are allowed to rotate, each having one rotational degree of freedom. The result of rotation of one or more wing tip bars is that the wings in which the rotated bars are connected to are tilted out of the sail plane spanned by the sail booms. Symmetrically tilting the wings can generate an attitude torque in the sail spin direction. The tilted wings method can be used in combination with other attitude control methods which lack a spin torque generation mechanism. For example, the tilted wing method was studied in combination with the shifted wings method by Wie [35] for the Jet Propulsion Laboratory New Millennium Program Space Technology 6 mission.

3.2.6. Billowed wings method

The billowed wings method (also referred to as tip displacement method) for solar sail attitude control was recently developed by Fu and Eke [36]. A square solar sail with four reflective triangular membranes (shown in Fig. 15) is used to illustrate this method. Each piece of triangular membrane, referred to as a wing, is connected to the booms at the apex of the triangle. The basic idea is to change the position of the wing attachment points (or boundary conditions of the wing membrane), such that the wing will billow under SRP to a new position. One possible billowed wings configuration which consists of two billowed wings when two tip connection points are moved a distance δ is shown in Fig. 15.

Notice that for any solar sail, the sail membrane will have a slight billow due to SRP. However, in the billowed wings method the degree of billowing is considerably larger and is controlled by moving the wing-boom attachment points. Originally, the cm and cp of the sail are at the center point *O* of the sailcraft. As the wing billows, the cm and cp of the membrane shifts. Controlled billowing of the wing leads to a controlled motion of the cm and cp of the membrane. This results in a body torque in all three major body axes directions that could be used for attitude control of the craft. For the wing billowing configuration shown by Fig. 15, the cp shifts to a new position, shown by a cross, and a body torque is generated as a result of the cm and cp shift. Notice that only one configuration is shown in this paper. By moving one or more of the wing tips of the four wings, it is possible to perform attitude maneuvers in all three major axes directions. Interested readers can refer to Ref. [36] for a detailed mathematical treatment of the wing model and attitude torque and tip displacement relationships.

The wing tip displacement method for solar sail attitude control is simple and does not require complicated mechanisms for implementation, thus improving weight efficiency of the solar sail over all. This method especially favors large sails, as the attitude control system mass can be a significant portion of the entire sail mass for many of the other types of attitude control system. Because this method relies on a curved sail profile, it might be inappropriate for small solar sails, as sail geometry can differ considerably from the desired configuration due to wrinkling. A mathematical model of an entire sail has been constructed to investigate the controllability of the sail [73]. Further investigation of the theoretical shape of the billowed sail membrane is presented in Ref. [74]. This method deserves further study because it is a promising attitude control method for very large solar sails. Further work is needed to understand membrane dynamics under SRP as membrane boundary conditions change.

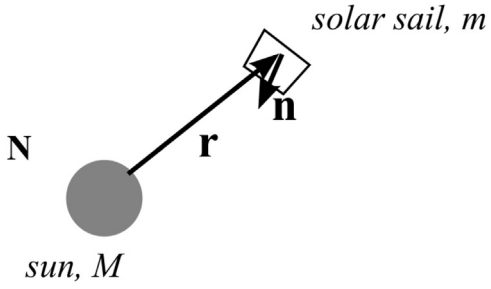

Fig. 18. Solar sail in inertial frame *N*.

Please cite this article as: B. Fu, et al., Solar sail technology—A state of the art review, Progress in Aerospace Sciences (2016), http://dx.doi.org/10.1016/j.paerosci.2016.07.001

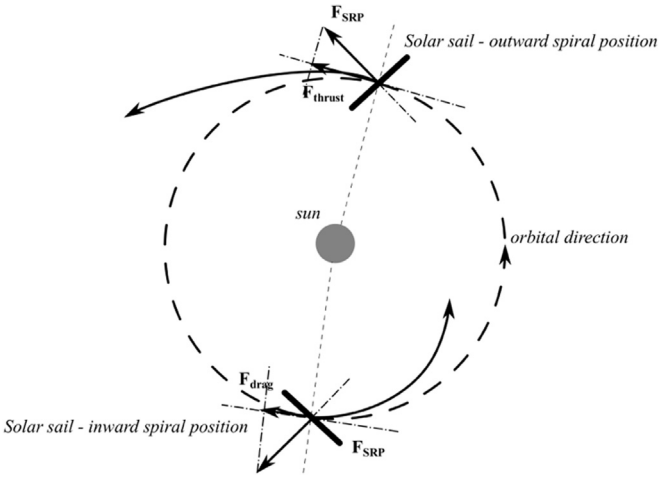

Fig. 19. Solar sail spiral trajectories.

3.3. Attitude control method for non-rigid sailcraft

3.3.1. Sail film with controllable reflectivity method

For non-rigid sailcraft whose shape is maintained by internal tension generated from centrifugal forces as a result of sail spin, attitude control methods for rigid sailcraft may not be applicable or may be ineffective. The lack of structural rigidity forbids any mechanism that puts a large out-of-plane load on the sail membrane. Notice that since rigid sailcraft can have a spin, attitude control methods for non-rigid sailcraft may be applicable to rigid sailcraft. Non-rigid sailcraft attitude control systems need to generate a body torque effectively while the sailcraft spins. Periodic attitude action is needed, and none of the previously discussed attitude control methods applies in this case. In the case of rigid sailcraft, one can move either the craft's cm or cp to generate a torque for attitude control purposes. However, for non-rigid sailcraft, moving the cp is the only practical option available. It would be unwise to move the cm off the spin axis as this could change the effective spin axis and possibly even the spin plane.

Alternatively, an attitude control method which uses reflectivity controlled membranes was developed for non-rigid sailcraft. Consider a spinning sailcraft shown in Fig. 16. The outer regions of the sail membranes are covered with a layer of membrane material whose transmissivity changes depending on the voltage applied. The coated sail membrane with the necessary electronics is referred to as a reflectivity control device in Fig. 16. When no voltage is applied, the coating material is not fully transparent, leading to a diffuse reflection dominated sail membrane. When a voltage is applied (indicated by device 'on'), the transmissivity of the coating material increases and the membrane becomes transparent. The overall effect is a specular reflection dominated reflective sail membrane. By changing the applied voltage of the reflectivity control device, sail reflectivity control is obtained. Since specular reflection and diffuse reflection generate different SRP forces, sail cp can be shifted out of the normal position which normally coincides with sail cm at the center point *O*. For example, in Fig. 16 the bottom right wing's reflectivity control device is in the 'off' state, while all the others are in the 'on' state. The overall result is a shift of cp (indicated by a cross), which results in a body torque **T** as shown. As the sail spins, periodically changing the on and off state of the available reflectivity control devices would allow a control torque to be generated in a fixed direction. By using reflectivity control devices, periodic attitude action can be performed without having any parts of the sail move in a periodic manner. The SRP force generated by changing surface reflectivity is very small, and out-of-plane load is considered acceptable. Notice that in the case the sail is perfectly flat, a spin torque cannot be generated by controlling the reflectivity of the sail membranes. Fig. 16 shows only four pieces of reflectivity control devices each located on a sail wing. For a real solar sail such devices usually consist of many smaller pieces which can be controlled separately.

The controllable reflectivity attitude control method was first developed by the Japan Aerospace Exploration Agency and was successfully demonstrated on the sailcraft IKAROS. Details of the attitude controller design and experimental data from attitude maneuver tests can be found in Ref. [64].

3.3.2. Attitude control for heliogyros

Consider a heliogyro solar sail with four blades spinning with constant angular speed ω, as shown in Fig. 17. The rotation of each blade about its axis can be controlled separately either at the outer tip or at the inner tip of the blade, and blade rotation angle, or pitch angle, is denoted by θ_{b_i}, with $i = 1, 2, 3, 4$ indicating blade number. Thus the system has four control degrees of freedom. The cm of the heliogyro stays at the center point *O* and does not move. Pitching a blade will change the SRP force experienced by that blade, and pitching all four blades collectively can produce a three axis body torque, as shown by **T** in Fig. 17. Periodically altering the pitch angles of the blade will provide a body torque for attitude control. For heliogyro attitude control studies it is generally assumed that the spin speed is much larger than the desired attitude maneuver speed, and the body torque generated is generally averaged over each period of rotation.

The simplest heliogyro dynamics model considers sail blades to be rigid. However, heliogyro blade length to width ratio can be very high, and blade structural dynamics, such as blade twist and bending, become non negligible. Blomquist [75] reviewed several heliogyro blade models and studied heliogyros with blade length to width ratio of 1000. NASA's finding on heliogyro structural dynamics using a Finite Element (FE) approach was reported by Wilkie et al. [76], which showed no intractable stability or control

Table 2
Solar sail projects and proposed solar sail missions.

Solar sail projects/missions	**Sail type**	**Sail size** (m^2)	**Development stage**
Illinois CubeSail [89]	Non-rigid	20	Ground test
LightSail-1 [90]	Rigid-square	32	Deployed in orbit
NanoSail-D [91]	Rigid-square	10	Ground test
NanoSail-D2 [92]	Rigid-square	10	Deployed in orbit
IKAROS [64]	Non-rigid	196	Sailed on SRP
GeoSail [93]	Rigid-square	1849	Conceptual
GeoStorm [5]	Rigid-square	4489	Conceptual
Solar pole orbiter [94,95]	Rigid-square	22,500	Conceptual
Intestellar Heliopause Probe [96]	Rigid-square	60,000	Conceptual
Sunjammer [97]	Rigid-square	1200	Ground test
Gossamer deorbit sail [98]	Rigid-square	25	Ground test

Please cite this article as: B. Fu, et al., Solar sail technology—A state of the art review, Progress in Aerospace Sciences (2016), http://dx.doi.org/10.1016/j.paerosci.2016.07.001

issues for the heliogyro. For a practical heliogyro, Guerrant and Lawrence [77] presented several pitching methods and ways to combine them to generate the desired attitude control torque.

3.4. Passive attitude stability

Spin stabilization is being discussed as a potential candidate for sailcraft during some or all phases of a variety of missions [18,23,34,78]. Thrust vector misalignment is typically considered as the major motivator for this. Sail shape uncertainty or manufacturing defects may produce an offset of the cp from its intended location, thereby inducing a constant body-fixed torque about the spacecraft cm. In the absence of some form of control, the sailcraft may begin to tumble. Wie [34] showed that spin stabilization will lead to nutation and precession of a sailcraft spin axis based on the usual dynamics of a spinning axisymmetric rigid body subject to a constant body-fixed torque. The amplitudes of the deviations are proportional to the cm/cp offset distance while the coning rates are proportional to the spin rate. Van der Ha and Lappas [78] proposed a model for studying the long-term attitude effects of solar radiation torques on a spinning spacecraft with reflective surfaces and constant cm/cp offsets. They concluded that the total disturbance torque acting on a spinning body is the time-averaged sum of the torques acting on each reflective subsurface of the spacecraft. Gong et al. [18] developed a model for studying the attitude stability of a slowly spinning conical sail in an elevated heliocentric orbit. The sail geometry is specifically chosen to counter the effects of the gravity gradient in addition to maintaining the orbit's position above the plane of the ecliptic. They pick a model that takes into account attitude-orbit coupling and demonstrate both analytically and numerically that orbit station keeping can be performed by giving the sailcraft a constant angular velocity about its symmetry axis. Lawrence et al. [23] develop a method for stabilizing the attitude of a sailcraft in a low altitude planetary orbit. They allow the spacecraft to cone about the orbit's local horizontal axis and determine configuration parameters that will cancel aerodynamic, gravitational, and solar radiation disturbance torques. This allows them to identify body spin rates that permit the spacecraft to maintain marginal pointing stability. Active control will then only be required to reduce the nutation angle.

4. Solar sail orbital dynamics and control

4.1. Equations of motion in sun centered orbit

Consider a system consisting of the sun with mass M and a solar sail with mass m, as shown in Fig. 18. $\mathbf{r} = r\mathbf{n_s}$ is a position vector from the sun's cm to the sail's cm, and $\mathbf{n}$ is a unit vector orthogonal to the sail directed toward the sun. Since $M \gg m$, the cm of the sun–sail system can be assumed to be at the sun's cm and gravitational acceleration on the sun can be neglected. An inertial reference frame, N, can be constructed in which the position of the sun does not change. The equation of motion of the sail can then be derived in N. Assume the only forces acting on the sail are gravity force $\mathbf{F}_g$ and SRP pressure force $\mathbf{F}_{SRP}$:

$$\mathbf{F}_g + \mathbf{F}_{SRP} = m\frac{d^2}{dt^2}\mathbf{r} \tag{43}$$

Using Eq. (34) and expressing the forces in terms of vectors $\mathbf{n_s}$ and $\mathbf{n}$, Eq. (43) becomes:

$$-\frac{GMm}{r^2}\mathbf{n_s} - 2PA(\mathbf{n_s}\cdot\mathbf{n})^2\mathbf{n} = m\frac{d^2}{dt^2}\mathbf{r} \tag{44}$$

If one defines $\mu \triangleq GM$, Eq. (44) can be written in terms of the constants μ and β:

$$\frac{d^2}{dt^2}(r\mathbf{n_s}) + \frac{\mu}{r^2}\mathbf{n_s} + \frac{\mu\beta}{r^2}(\mathbf{n_s}\cdot\mathbf{n})^2\mathbf{n} = 0 \tag{45}$$

Planar motion of the sail in a sun centered orbit is illustrated in Fig. 19. Depending on how the sail is tilted, a component of $\mathbf{F}_{SRP}$ can point either in the direction or opposite the direction of motion. The consequence is a spiral trajectory which depends on the sail orientation. In the outward spiral case the sail orbital velocity is constantly increased, while in the inward spiral case the sail orbital velocity decreases, essentially causing the sail to 'fall' into the sun.

4.2. Solar sails: the three body problem

Prediction of motion of three massive bodies (assumed to be point masses) under the effect of mutual gravitational attraction is commonly referred to as the three body problem. The dynamics of such systems is quite rich, but usually relies on several simplifying assumptions to arrive at tractable solutions. When considering a spacecraft as part of a three body system, the mass of the spacecraft is generally much smaller than the other two primary masses. Constraints, such as circular or elliptic planar motion, can be imposed on the primary masses in restricted three body problems. Around the primary masses, there are locations—the Lagrangian points—at which the spacecraft can remain at an equilibrium with respect to the two primary masses. For a solar sail, in addition to gravitational forces, SRP forces have to be accounted for in the determination of Lagrangian points. The fact that SRP forces are dependent on the orientation of the craft introduces some complexity to the problem. For the sun–earth–sail three body system, McInnes [5] presented a summary of the system equations of motion which take into account the orientation of the sail. He discussed in detail possible sail trajectories, including non-Keplerian trajectories. Highly-non-Keplerian Orbits for solar sail, among many other low-thrust propulsion techniques, were reviewed by McKay et al. [79]. In the case of a solar sail whose normal direction is directed along the sun line, McInnes et al. [80] showed that based on sail loading, new artificial equilibrium points existed around the classical Lagrangian points in the circular restricted three body problem (CR3BP). The design of transfer trajectories between Earth and equilibrium points, and between equilibrium points using invariant manifolds have been presented by Gong et al. [21]. The classical halo periodic orbit around the artificial sun–earth L_1 Lagrangian point has been studied by Baoyin and McInnes [31]. The local dynamics of the halo orbit around the artificial L_1 is studied further by Farres and Jorba [22,81], where the influence of sail attitude change is considered. The evolution of possible halo orbits for solar sail of different sail

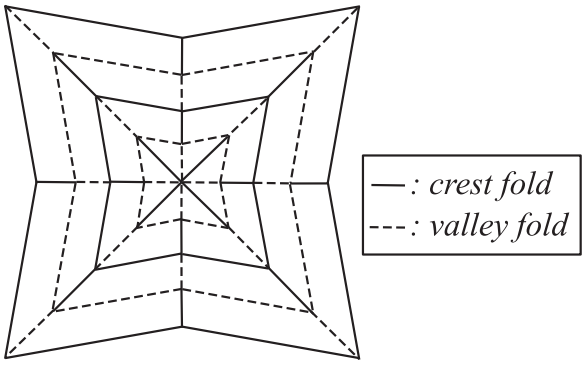

Fig. 20. An example of a tree leave folding pattern.

Please cite this article as: B. Fu, et al., Solar sail technology—A state of the art review, Progress in Aerospace Sciences (2016), http://dx.doi.org/10.1016/j.paerosci.2016.07.001

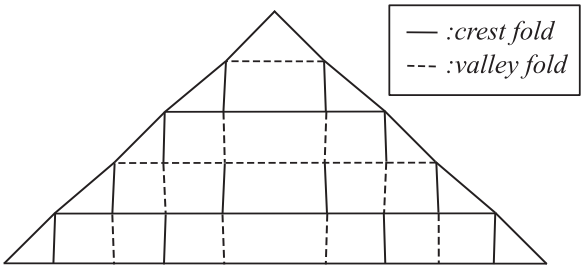

Fig. 21. Frog leg folding pattern.

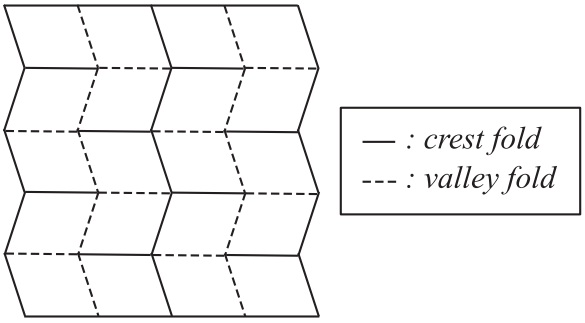

Fig. 22. Miura-ori folding pattern.

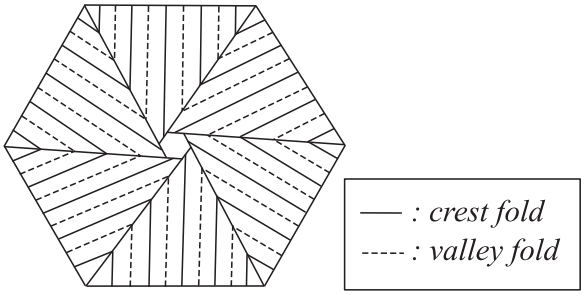

Fig. 23. Spiral folding pattern.

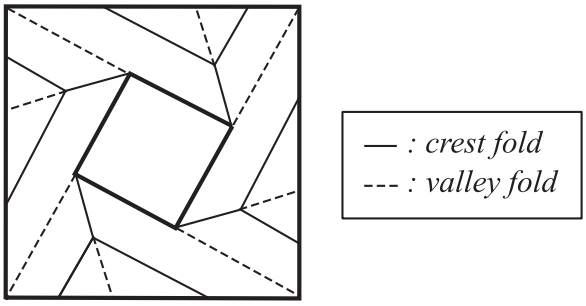

Fig. 24. Modified spiral folding pattern.

lightness number β has been studied by Verrier et al. [82] using boundary-value problem numerical continuation methods, where bifurcations are observed as values of β are increased. Other possible periodic orbits in the solar sail CR3BP have been pointed out by Waters and McInnes [30,83]. Solar sails in the elliptic restricted three-body problem (ER3BP) have been studied in some depth by Baoyin and McInnes [84] and later by Aliasi et al. [85], where the stability of artificial equilibrium points is discussed. Control related issues for a solar sail in CR3BP have been addressed by Waters and McInnes [86], where transfer from Earth and between fixed points missions are used as a demonstration. Similar to the way SRP generate artificial equilibrium points in the sun–earth–sail three body system, artificial equilibrium points are also present for other three body systems that involve SRP. For example, solar radiation pressure would generate artificial equilibrium points for a solar balloon in the α Centauri binary star system [13].

4.3. Orbits, trajectories and missions

Historically, solar sail orbits and trajectories have attracted much attention, and studies of solar sail orbits precede studies of other aspects, such as sail design and attitude dynamics. Solar sail's orbits and trajectories are much richer compared to traditional spacecraft. There are two main reasons for this. One is that a solar sail is continuously under thrust. This allows it to accumulate a large velocity change (ΔV) over time, making it suitable even for large ΔV missions. Another reason is that the continuous thrust can be directed in a way that allows a solar sail to enter orbits that are non-Keplerian. Theoretically, a solar sail has the potential to reach any part of the solar system and even beyond. The low and continuous thrust of a solar sail allows it to remain gravitationally stable at locations that cannot be maintained by conventional spacecraft. A solar sail can remain in a stationary position that is sunward of the earth Lagrangian point (L_1 point). Such a solar sail can be used to monitor solar activity, and can give early warning of geomagnetic storms compared to a conventional spacecraft that can only remain stationary at L_1 (see Geostorm mission concept [5]). A solar sail can also be located at stationary positions directly below or above a planetary body. Trajectories for a solar sail Lunar south pole coverage have been investigated by Ozimek et al. [24]. A high performance solar sail could even be stationed above the poles of the Earth (see Polesitter concept [5,87]), enabling continuous observation of the polar regions of the Earth. A detailed trajectory and design analysis for a pole-sitter mission were carried out by Ceriotti et al. [45].

Macdonald and McInnes [88] presented a mission catalog based on the difficulty level of proposed solar sail missions and suggested a roadmap for solar sail missions. This catalog serves as a guide to future solar sail mission directions. A list of recently proposed solar sail missions is presented in Table 2. Most proposed solar sail missions use a rigid square solar sail, with size ranging from several square meters to several thousand square meters. So far both the IKAROS and the LightSail were successfully launched while all other proposed missions are either at ground test stage or in conceptual stage. The NanoSail-D mission failed due to a launch vehicle failure and the Sunjammer mission was terminated after failing critical technical review before planned launch in 2015. The GeoSail mission uses a solar sail to enable long residence times in the Earth's magnetotail [88,99]. A design of a lightweight sail suitable for the GeoSail mission concept has been presented by Lappas et al. [47]. Note that planet centered solar sailing may require fast slew rates, and is hence unattractive. However, missions such as GeoSail (or Mercury Sun-Sync mission [100]) do not require fast slew rates.

Solar sails could also be used in sample retrieving or rendezvous missions [33,54,101–103]. The effectiveness of solar sailing is truly shown by its high ΔV capabilities. For example, a system and trajectory analysis for a sample return mission to Mercury [102] showed significant reduction in launch mass and mission duration. This also improves cost effectiveness of the overall mission. A preliminary study by Mengali and Quarta [43], assuming circular and coplanar planetary orbits, showed the feasibility of using solar sails as stopover cyclers for cargo transportation missions. Large solar sails could potentially serve as cargo transporters for future space missions [36]. The interaction between solar sails and asteroids is another focus of study in solar sail trajectory analysis [33,48,54,104–107]. Near earth interplanetary space contains asteroids that can potentially be mined for resources. The technical and economical aspect of asteroid mining have been studied in the literature [108,109]. Major cost issues involved with transportation

Please cite this article as: B. Fu, et al., Solar sail technology—A state of the art review, Progress in Aerospace Sciences (2016), http://dx.doi.org/10.1016/j.paerosci.2016.07.001

of mined resources can potentially be reduced by the use of solar sails. If successful, reduction of space mining cost can boost human space activity significantly. Solar sails have also been proposed as candidate gravity tractors for asteroid deflection, taking advantage of the propellantless nature of solar sailing. The practical viability has been shown for a deflection mission for the asteroid Apophis by Wie [104], and a formation flying scheme that uses many solar sails to deflect near earth asteroids has been proposed by Gong et al. [107].

For a solar sail, operation near planetary bodies where other space environmental forces, such as atmospheric drag and magnetic forces, are significant should be avoided. Near earth, solar sails are thought to be inappropriate for orbits below an altitude of 750 km [110]. Although active solar sailing could provide a means to de-orbit a spacecraft nearing the end of its operational life [89,111], it is inefficient compared to other de-orbiting methods, such as using existing propulsion system on board the craft [112]. Alternatively, solar sails could be used as fail-safe devices to passively de-orbit spacecraft in high altitude orbits [113]. It is important to note that solar sails are fragile and hence operation near planetary bodies should be planned carefully if inevitable.

The high ΔV potential of solar sails makes them suitable candidates for interstellar missions, such as the Interstellar Heliopause Probe [96,114] and a beryllium hollow-body solar sail [115]. For solar sails interstellar missions it is favorable to allow the craft to gain energy by first coming close to the sun. Some optimal trajectories for such missions have been studied by Dachwald [52]. In this work it is assumed that only gravitational forces and radiation pressure forces act on the solar sail. Minimal sun–sail distance as well as maximum allowed sail temperature has been considered as constraints for trajectory optimization.

In the literature, solar sail trajectory estimation is commonly based on simple solar sail models which consider the sail to be rigid with solar radiation pressure force that is simply a function of time. However, there are many factors that can cause actual trajectories to deviate from the predicted trajectories, including structural dynamics of the sail, sail optical property changes and sail temperature variations. During a solar sail's operational life, the elastic deformation of the sail can have an effect on sail thrust, hence influence sail trajectory. Ingrassia et al. [41] used a FE approach to estimate how sail trajectory is influenced by sail elastic deformation. Using their FE model, impact of incomplete sail deployment on sail trajectory is also studied. An Earth–Venus interplanetary transfer trajectory is then used to demonstrate the significance of solar sail structural dynamics on the estimated sail trajectory. Optical properties of sail membranes can degrade over time. The impact of sail optical property degradation on sail trajectory has been investigated by McInnes [60]. Using the optical degradation model developed by Dachwald et al. [59,116], and assuming purely specular reflection and constant emissivity of the sail, McInnes presented a closed-form solution to the solar sail spiral trajectory for sails with time-varying reflectivity. As solar sail trajectories pass close by the sun, the drag force caused by Poynting–Robertson effect could become large and therefore not negligible. Kezerashvili and Vázquez-Poritz [42] studied this drag force for a sun sail distance between 0.02 au and 0.38 au, and found that it can reduce orbital velocity, causing the craft to slowly spiral toward the sun.

5. Practical solar sailing

5.1. Solar sail packaging and deployment

Designing a solar sail is quite a tricky task. A solar sail cannot escape from the earth's atmosphere by itself, therefore it would need to be first packed into a reasonable size to fit into a launch vehicle. After it is released from the launch vehicle, it would need to fully deploy to a functional sailcraft. A spin type sail, such as the IKAROS, has no structural support components and relies on centrifugal forces from the spinning of the craft to deploy. Other spin deployed solar sail concepts include the MacNeal heliogyro [63] and its variation concepts [117–119]. A solar sail with rigid support boom does not need a spin force for deployment, and the sail can deploy either together with the booms or after the boom, based on a rope mechanism (see the ODISSEE project [120]).

One of the design challenges for both spin and non-spin solar sails lies in the effective packaging of the entire sail membrane into a small volume. For the heliogyro, the folding problem is much simpler, as the sail consists of membrane blades that are simply rolled. Other solar sails with different membrane geometries will face more difficulty when packaging. Interestingly, nature has provided a packaging solution. Young tree leaves are folded inside small buds before they deploy and mature. Similar folding patterns as shown in Fig. 20 can be used to effectively fold solar sails [121]. Knowledge of the art of origami could also provide insight into effectively folding of solar sails. For triangular membranes, such as the ones used as a quadrant of a square solar sail, the so-called 'frog leg' packaging method [122] has been proposed (see Fig. 21). A similar folding method is the folding pattern adopted on the Surrey CubeSail [123]. Other folding patterns, such as the Miura-ori folding pattern shown in Fig. 22, could also be effective in folding an entire square solar sail. Papa and Pellegrino [124] have studied a square Kapton membrane that is deployed from an originally folded state using a Miura-ori pattern. Attention was given to the crease angle and stress levels of the deployed membrane and the corner forces which stretch the square membrane. Another common folding pattern which can be used is the spiral folding pattern, where a flat sail is folded around a central hub. An example of such a pattern is shown in Fig. 23. A modified version of the spiral folding pattern (see Fig. 24) was suggested by Banik and Murphey in their study of the deployment of a rigid square solar sail [125]. The shape of such a sail was later experimentally validated using photogrammetry [126].

Deployment dynamics is also an area of interest for solar sail designers. Understanding sail deployment dynamics, both theoretical and experimental, is critical for successful sail deployment and future sail designs. Salama et al. [127] presented an experimental investigation of a spin deployed solar sail concept originally intended for the Interstellar Probe Mission. Although most solar sails are square shaped, other sail shapes, such as hexagon shaped membranes, are viable. The centrifugal deployment of a hexagonal membrane has been studied by Okuizumi and Yamamato [128]. Deployment experiments for both a coarse and fine spiral folding pattern (see Fig. 23) performed in a vacuum chamber showed that such membranes could be smoothly deployed in a matter of seconds. However their experiments also showed that in and out of plane vibrational modes were excited, and suppression of such vibrations is critical for the stability of the spinning solar sail. Perhaps polymer based damping material could be attached throughout the deployment phase in order to quickly damp out the unwanted out of plane vibrations.

For solar sails that have structural booms for support, reliable mechanisms for boom deployment are important. Although the purpose of sail booms is to maintain structural support, they may not need to be very stiff since the load on a solar sail is typically small. Sail booms can be deployed by a variety of ways including a telescopic mechanism, rigid linkage mechanism, inflatable mechanism, or reeling mechanism. For small solar sails, weight, reliability and structural complexity issues seem to favor the reeling deployment mechanism. Sail booms are typically made out of lightweight composite materials which are stable in both the

Please cite this article as: B. Fu, et al., Solar sail technology—A state of the art review, Progress in Aerospace Sciences (2016), http://dx.doi.org/10.1016/j.paerosci.2016.07.001

packed and deployed configurations. The strain energy in the packed state can be used to provide forces for deployment, such as the booms used on the Nanosail-D solar sail (trac booms [91]) and the Surrey CubeSail (Bi-Stable composite booms [129]). Electrical drives can also provide the needed force for deployment, as shown by the carbon-fiber reinforced polymer booms (CFRP booms [130]) developed by DLR. CFRP booms consist of two Omega shaped half-shells (see figure) which form a tube like structure. Although the booms can be deployed using electrical drives attached to the boom ends, adding a polymer bladder inside the tube structure creates an inflatable mechanism for deployment [131]. Boom buckling, jamming and other issues that could lead to deployment failure are of concern, and zero-*g* flight tests were performed to verify the deployment mechanism of the CFRP booms.

Generally, larger solar sails would require booms with extreme length-to-diameter ratios. Single piece booms developed for small sails may be insufficient to provide the needed structural support and mass effectiveness for large sails. Issues involved in scalability of solar sail designs have been reviewed by Greschik [132]. He pointed out that recognition of surface shape contribution to sail scalability is critical, and that careful attention should be paid to model assumptions to increase reliability, especially when affordable physical verification is impossible at large dimensions. A coilable design which consists of an assembly of carbon-fiber longerons was developed by Murphy et al. [68] and could potentially scale up to a length of up to 100 m. Based on the coilable design, the Superstring concept was later developed by Brown [133]. This assembly features efficient packaging, mass effectiveness as well as increased bending strength, providing an engineering solution for solar sails whose structural mast is up to 1000 m in length. For a heliogyro type sail and its variations, deployment is achieved through the unreeling of sail blades. The peel force (the force needed to peel one layer of film from another) involved in the unreeling process was experimentally studied in a vacuum chamber by Woo et al. [117].

On the other extreme, solar sails can be very small, and the packaging and deployment issues involved could be less demanding. Lappas et al. [134] proposed a 5 m by 5 m solar sail with integrated sail membranes and booms, and whose deployment can be achieved through simple inflation, thus reducing deployment system complexity. Inspired by dust particles in space, Atchison and Peck [46] proposed a solar sail that is in the millimeter length scale. The entire sail could be built on a 1 cm^2 silicon substrate, and deployment is not needed at all.

5.2. Structural dynamics

Understanding the structural dynamics of solar sails is necessary for a good solar sail design. Structural deformation from external and internal load could lead to diminished sail performance or even sail disintegration. Possible vibratory motion of the sail can lead to instability, and should be kept within acceptable levels. Since solar sails vary considerably in size and configuration, it is best to refer to a specific solar sail for any in depth discussions regarding the structural dynamics of solar sails. Cassenti et al. [135] presented a study of a class of parachute type interstellar solar sails. They reviewed membrane and plate theories that can be applied to study solar sail membrane structures. However, in the literature a rigid type square solar sail with structural booms has been used as a reference sail. In the following discussions on solar sail structural dynamics, such a reference sail is omitted.

Many have used FE based methods to model a solar sail. Building up from first-order, 3-D Timoshenko beam elements, Stanciulescu et al. [136] studied the entire support structure of a square solar sail. Attention was given to beam vibration and buckling. Another solar sail structural model using FE method was developed by Genta et al. [137]. Due to the large length to thickness ratios of sail membranes, standard general purpose FE codes failed to yield consistent results, and specialized FE codes that could model thin flat membranes had to be developed. To prevent tear propagation, sail membranes with ripstops are considered.

Liu et al. [138] studied large scale sail boom vibration using a Euler–Bernoulli beam model. Forces from attitude control mechanisms, such as sliding mass and control vanes are considered. Expected changes in vibratory responses from sliding masses have been observed through numerical simulations. Gaspar et al. [139] presented an experimental solar sail structural test program at NASA. The tests included vibration modal test in vacuum environment and shape testing using photogrammetry.

Solar sail membrane fluttering has been studied by Gibbs and Dowell [140]. They analyzed a membrane section of the Sunjammer solar sail, and found that small limit-cycle oscillations, in the order of the thickness of the membrane, are expected. Unlike other flexible space structures, wrinkling in sail wings can directly cause sail performance problems, and should be considered for high fidelity sail models. Membrane wrinkling caused by asymmetric pre-stressed loading at the corners of a square membrane has been studied by Wong and Pellegrino [141]; they built analytical and theoretical models to characterize and predict wrinkles. Their analytical model was compared with an FE model and validated against experimental data. A thorough discussion on the topic of membrane wrinkling by Wong and Pellegrino can be found in Refs. [142,143]. Determination of the minimal thickness of metallic foil required for a solar sail to achieve maximum reflection and absorption of solar radiation can aid the design of solar sail membranes, especially material selection. Kezerashvili [144,145] showed that this minimal membrane thickness depends on the radiation wavelength and temperature of the material, and discussed minimal thickness cases for Aluminum and Beryllium coating.

6. Discussion and future perspectives

The success of the IKAROS solar sail is the beginning of a new era for solar sailing. Unlike most other spacecraft, many solar sails cannot be effectively tested on the ground because of their sizes. Several reasons for this and other dimensionality problems involved in solar sail design have been discussed by Greschik [132]. Hence, mathematical modeling and simulations are commonly used in solar sail studies, without any experimental validation. Hence, one must pay close attention to the assumptions made, as inappropriate assumptions drastically reduce the reliability of the findings.

There are a number of SRP force models developed for solar sails, each with different assumptions and accuracy. A quantitative comparison of these models would be an interesting area of future study. There are still many aspects of this topic that have not been studied in detail. One of those is shadowing, whether it is by a planetary object or by other parts of the sail. Shadowing not only reduces thrust capabilities, but can also significantly reduce the effectiveness of any attitude control system which relies on the cm/cp offset concept. Loss of attitude control capabilities would be very dangerous for any spacecraft. Self-shadowing is often neglected in sail models. Including self-shadowing effects is not simple, and determination of self-shadowing regions can be computationally prohibitive [65]. Since some solar sails are not flat by design, or have wrinkles, solar radiation can be reflected by many parts of the sail before being redirected back to space. In order to model such an effect one must consider radiation energy distribution by frequency. This multi-reflection effect can alter cp location, causing a disturbance in sail attitude.

Please cite this article as: B. Fu, et al., Solar sail technology—A state of the art review, Progress in Aerospace Sciences (2016), http://dx.doi.org/10.1016/j.paerosci.2016.07.001

As the sun–sail distance changes, the temperature of the sail, which is a result of an energy equilibrium, also changes. For a sail that is tilted at an angle with respect to the sun, the temperature distribution is non-uniform, and cooler regions tend to sag less than hotter regions due to non-uniform thermal expansion. Although it is well known that thermal issues affect the shape of the sail [125], its overall effect on sail trajectory has not been thoroughly studied. Solar sail geometry variations due to temperature changes can play a significant role in sail trajectory estimation, especially for trajectories that range from close to the sun to far away from the sun. Since many optical parameters are temperature dependent, an iterative process will be needed if temperature distribution is not considered uniform. All of the above add a degree of complexity to sail modeling. The level of complexity to which a sail model should be developed should really be decided on a case-by-case basis.

A number of attitude control systems based on the cm/cp displacement idea have been reviewed in this paper. There are a number of considerations for choosing an appropriate attitude control method for a solar sail mission. First is control redundancy. For example, a four vaned solar sail would have a higher degree of control redundancy compared to a single gimbaled solar sail. This is because the four vaned case is still likely to have attitude control authority even when one of the control vanes malfunctions, compared to a total loss of control authority in the case where the gimbal device fails. Second is sail size and mass. The attitude dynamics and control of a solar sail whose payload is located at the center hub can differ considerably from one with its payload mass at other parts of the sail. A change of cp location will be much easier to achieve compared to position change of cm (which will likely stay close to the center). Attitude control methods that shift the cp, such as the shifted wings method or the billowed wings method would thus be more appropriate for sailcraft with its payload concentrated at its center hub. In the case where payload mass is used as control mass, one has to also provide for the situation when the payload is dropped at the destination. The sail without payload must still be capable of attitude control. The last is design complexity. A structurally more complex solar sail would be more difficult to deploy compared to a solar sail with a simple design. Sail structural dynamics and membrane dynamics are also interesting areas for future study.

The future of solar sailing is bright. A key benefit solar sails can potentially offer is cost reduction. Potential cost reductions for Mars cargo missions were briefly discussed by Wright [4]. Affordability would likely be a major issue in humanity's future space program development. Solar sail's ability to achieve high ΔV missions with low cost can significantly reduce the cost of interplanetary missions. The possibilities of a hybrid design that consists of a solar sail that also includes an electric propulsion system has been discussed [88,146–148], and may provide benefits beyond those that come from using only solar radiation propulsion. New time effective mission trajectories could arise for such hybrid sailcraft that can lead to further cost reduction. Looking through human history, cost-effective transportation promotes exploration. Further understanding and quantifying cost reduction by the use of solar sails are areas of interest for future work. In the 15th century, humanity sailed across the oceans. After six centuries, humanity is sailing in space.

References

[1] J. Kepler, Ioannis Kepleri mathematici Cæsarei Dissertatio cum Nuncio sidereo: nuper ad mortales misso à Galilæo Galilæo mathematico Patavino, H.F. Schulz in Kommission, Pragæ, M.DC.X, 1610.

[2] M. Urbanczyk, Solar Sails—A Realistic Propulsion for Spacecraft (NASA-TM-X-60560, RSIC-694), Technical report, NASA, 1965.

[3] F. Tsander, Problems of Flight by Jet Propulsion: Interplanetary Flights (F-147), Technical report, NASA, 1964.

[4] J.L. Wright, Space Sailing, Gordon Breach Science Publishers S.A., Philadelphia, US, 1992.

[5] C.R. McInnes, Solar sailing: technology, dynamics and mission applications, in: Springer Praxis Books/Astronomy and Planetary Sciences, Springer, Berlin, Germany, 2004.

[6] D.J. O'Shaughnessy, J.V. McAdams, K.E. Williams, B.R. Page, Fire sail: MESSENGER's use of solar radiation pressure for accurate Mercury flybys, in: 32nd Guidance and Control Conference, Paper AAS 09-014, American Astronautical Society, Breckenridge, US, 2009.

[7] A.A. Siddiqi, Deep Space Chronicle: A Chronology of Deep Space and Planetary Probes 1958–2000, Monographs in Aerospace History No. 24, NASA, 2002.

[8] J.M. Longuski, R.E. Todd, Survey of nongravitational force sand space environmental torques: applied to the Galileo, J. Guid. Control Dyn. 15 (3) (1992) 545–553.

[9] V. Koblik, E. Polyakhova, L. Sokolov, Solar sail near the sun: point-like and extended models of radiation source, Adv. Space Res. 48 (2011) 1717–1739.

[10] R.L. Forward, Gray solar sails, J. Astronaut. Sci. 28 (2) (1990) 161–185.

[11] Z. Kun, Control capability and allocation of solar sail tip vanes over bounded movement, J. Guid. Control Dyn. 38 (7) (2015) 1340–1344.

[12] K. Parsay, H. Schaub, Designing solar sail formations in sun-synchronous orbits for geomagnetic tail exploration, Acta Astronaut. 107 (2015) 218–233.

[13] G. Aliasi, G. Mengali, A. Quarta, Artificial equilibrium points for a solar balloon in the α Centauri system, Acta Astronaut. 104 (2014) 464–471.

[14] A. Farrés, A. Jorba, Station keeping of a solar sail around a Halo orbit, Acta Astronaut. 94 (2014) 527–539.

[15] J. Zhang, T.S. Wang, Coupled attitude-orbit control of flexible solar sail for displaced solar orbit, J. Spacecr. Rocket. 50 (3) (2013) 675–685.

[16] A.A. Quarta, G. Mengali, Optimal solar sail transfer to linear trajectories, Acta Astronaut. 82 (2013) 189–196.

[17] J. Mu, S. Gong, J. Li, Reflectivity-controlled solar sail formation flying for magnetosphere mission, Aerosp. Sci. Technol. 30 (2013) 339–348.

[18] S. Gong, J. Li, K. Zhu, Dynamical analysis of a spinning solar sail, Adv. Space Res. 48 (2011) 1797–1809.

[19] G.G. Wawrzyniak, K.C. Howell, Numerical techniques for generating and refining solar sail trajectories, Adv. Space Res. 48 (2011) 1848–1857.

[20] S. Gong, G. Yunfeng, J. Li, Solar sail formation flying on an inclined Earth orbit, Acta Astronaut. 68 (2011) 226–239.

[21] S. Gong, H. Baoyin, J. Li, Solar sail three-body transfer trajectory design, J. Guid. Control Dyn. 33 (2010) 873–886.

[22] A. Farrés, A. Jorba, Dynamics of a solar sail near a Halo orbit, Acta Astronaut. 67 (2010) 979–990.

[23] D.A. Lawrence, M.S. Whorton, Solar sail dynamics and coning control in circular orbits, J. Guid. Control Dyn. 32 (2009) 974–985.

[24] M.T. Ozimek, D.J. Grebow, K.C. Howell, Design of solar sail trajectories with applications to lunar south pole coverage, J. Guid. Control Dyn. 32 (2009) 1884–1897.

[25] J.D. Biggs, C. McInnes, Solar sail formation flying for deep-space remote sensing, J. Spacecr. Rocket. 46 (2009) 670–678.

[26] M. Xu, S. Xu, Structure-preserving stabilization for Hamiltonian system and its applications in solar sail, J. Guid. Control Dyn. 32 (2009) 997–1004.

[27] G. Mengali, A.A. Quarta, Solar sail trajectories with piecewise-constant steering laws, Aerosp. Sci. Technol. 13 (2009) 431–441.

[28] D.A. Lawrence, M.S. Whorton, Coning control of solar sails using magnetic momentum error reduction, J. Spacecr. Rocket. 46 (2009) 1298–1308.

[29] J. Bookless, C. McInnes, Control of Lagrange point orbits using solar sail propulsion, Acta Astronaut. 62 (2008) 159–176.

[30] T.J. Waters, C.R. McInnes, Periodic orbits above the ecliptic in the solar-sail restricted three-body problem, J. Guid. Control Dyn. 30 (2007) 687–693.

[31] H. Baoyin, C.R. McInnes, Solar sail halo orbits at the sun–earth artificial L 1 point, Celest. Mech. Dyn. Astron. 94 (2006) 155–171.

[32] G. Colasurdo, L. Casalino, Optimal control law for interplanetary trajectories with nonideal solar sail, J. Spacecr. Rocket. 40 (2003) 260–265.

[33] E. Morrow, D.J. Scheeres, D. Lubin, Solar sail orbit operations at asteroids, J. Spacecr. Rocket. 38 (2001) 279–286.

[34] B. Wie, Solar sail attitude control and dynamics, Part 1, J. Guid. Control Dyn. 27 (2004) 526–535.

[35] B. Wie, Solar sail attitude control and dynamics, Part 2, J. Guid. Control Dyn. 27 (2004) 536–544.

[36] B. Fu, F.O. Eke, Attitude control methodology for large solar sails, J. Guid. Control Dyn. 38 (4) (2014) 662–670.

[37] T. Yamaguchi, Y. Mimasu, Y. Tsuda, M. Yoshikawa, Hybrid estimation of solar radiation pressure for a spinning solar sail spacecraft, J. Spacecr. Rocket. 51 (1) (2014) 381–384.

[38] S. Gong, J. Li, Spin-stabilized solar sail for displaced solar orbits, Aerosp. Sci. Technol. 32 (2014) 188–199.

[39] Y. Tsuda, T. Saiki, R. Funase, Y. Mimasu, Generalized attitude model for spinning solar sail spacecraft, J. Guid. Control Dyn. 36 (2013) 967–974.

[40] X. Hu, S. Gong, J. Li, Attitude stability criteria of axisymmetric solar sail, Adv. Space Res. 54 (2014) 72–81.

[41] T. Ingrassia, V. Faccin, A. Bolle, C. Circi, S. Sgubini, Solar sail elastic displacement effects on interplanetary trajectories, Acta Astronaut. 82 (2013) 263–272.

Please cite this article as: B. Fu, et al., Solar sail technology—A state of the art review, Progress in Aerospace Sciences (2016), http://dx.doi.org/10.1016/j.paerosci.2016.07.001

[42] R.Y. Kezerashvili, J.F. Vázquez-Poritz, Effect of a drag force due to absorption of solar radiation on solar sail orbital dynamics, Acta Astronaut. 84 (2013) 206–214.
[43] G. Mengali, A.A. Quarta, Solar-sail-based stopover cyclers for cargo transportation missions, J. Spacecr. Rocket. 44 (2007) 822–830.
[44] M. Ceriotti, C.R. Mcinnes, Generation of optimal trajectories for earth hybrid pole-sitters, J. Guid. Control Dyn. 34 (3) (2011) 847–859.
[45] M. Ceriotti, J. Heiligers, C.R. Mcinnes, Trajectory and spacecraft design for a pole-sitter mission, J. Spacecr. Rocket. 51 (1) (2014) 311–326.
[46] J.A. Atchison, M.A. Peck, A passive, sun-pointing, millimeter-scale solar sail, Acta Astronaut. 67 (2010) 108–121.
[47] V. Lappas, G. Mengali, A. Quarta, J. Gil-Fernandez, T. Schmidt, B. Wie, Practical systems design for an earth-magnetotail-monitoring solar sail mission, J. Spacecr. Rocket. 46 (2009) 381–393.
[48] G. Mengali, A.A. Quarta, Rapid solar sail rendezvous missions to asteroid 99942 apophis, J. Spacecr. Rocket. 46 (2009) 134–140.
[49] G. Mengali, A.A. Quarta, Solar sail near-optimal circular transfers with plane change, J. Guid. Control Dyn. 32 (2009) 456–463.
[50] S.M. Wokes, P. Palmer, M. Roberts, Classification of two-dimensional fixed-sun-angle solar sail trajectories, J. Guid. Control Dyn. 31 (2008) 1249–1258.
[51] G. Mengali, A.A. Quarta, In-orbit repositioning of multiple solar sail spacecraft, Aerosp. Sci. Technol. 12 (2008) 506–514.
[52] B. Dachwald, Optimal solar-sail trajectories for missions to the outer solar system, J. Guid. Control Dyn. 28 (2005) 1187–1193.
[53] B. Dachwald, B. Wie, Solar sail trajectory optimization for intercepting, impacting, and deflecting near-earth asteroids, in: AIAA Guidance, Navigation and Control Conference and Exhibit, AIAA, San Francisco, California, http://dx.doi.org/10.2514/6.2005-6176, 2005.
[54] B. Dachwald, W. Seboldt, Multiple near-Earth asteroid rendezvous and sample return using first generation solar sailcraft, Acta Astronaut. 57 (11) (2005) 864–875.
[55] L. Rios-Reyes, D.J. Scheeres, Generalized model for solar sails, J. Spacecr. Rocket. 42 (1) (2005) 182–185.
[56] L. Rios-Reyes, D.J. Scheeres, Solar-sail navigation: estimation of force, moments, and optical parameters, J. Guid. Control Dyn. 30 (3) (2007) 660–668.
[57] G. Mengali, A.A. Quarta, C. Circi, B. Dachwald, Refined solar sail force model with mission application, J. Guid. Control Dyn. 30 (2007) 512–520.
[58] G. Vulpetti, S. Scaglione, Aurora project: estimation of the optical sail parameters, Acta Astronaut. 44 (2-4) (1999) 123–132.
[59] B. Dachwald, G. Mengali, A.A. Quarta, M. Macdonald, Parametric model and optimal control of solar sails with optical degradation, J. Guid. Control Dyn. 29 (5) (2006) 1170–1178.
[60] C.R. Mcinnes, Approximate closed-form solution for solar sail spiral trajectories with sail degradation, J. Guid. Control Dyn. 37 (6) (2014) 2053–2057.
[61] E. Sperber, Attitude dynamics and control of solar sails (Ph.D. dissertation), University of California, Davis, 2014.
[62] Y. Tsuda, Y. Okano, Y. Mimasu, R. Funase, On-orbit sail quality evaluation utilizing attitude dynamics of spinner solar sailer IKAROS, in: Advances in the Astronautical Sciences, vol. 143, 2012, pp. 1609–1625.
[63] R. MacNeal, J. Hedgepeth, H. Schuerech, Heliogyro Solar Sailer: Summary Report, NASA Technical Report CR-1329, 1969.
[64] R. Funase, Y. Shirasawa, Y. Mimasu, O. Mori, Y. Tsuda, T. Saiki, J. Kawaguchi, On-orbit verification of fuel-free attitude control system for spinning solar sail utilizing solar radiation pressure, Adv. Space Res. 48 (2011) 1740–1746.
[65] M. Choi, C. Damaren, Structural dynamics and attitude control of a solar sail using tip vanes, J. Spacecr. Rockes, 52 (6), 2015, pp. 1665–1679, http://dx.doi.org/10.2514/1.A33179.
[66] M.B. Quadrelli, J. West, Sensitivity studies of the deployment of a square inflatable solar sail with vanes, Acta Astronaut. 65 (2009) 1007–1027.
[67] F. Angrilli, S. Bortolami, Attitude and orbital modeling of a solar sail spacecraft, ESA J. 14 (1990) 431–446.
[68] D.M. Murphy, T.W. Murphey, P.A. Gierow, Scalable solar-sail subsystem design concept, J. Spacecr. Rocket. 40 (4) (2003) 539–547.
[69] E. Sperber, B. Fu, F. Eke, Large angle reorientation of a solar sail using gimballed mass control, J. Astronaut. Sci. 63 (2), 2016, 103–123, http://dx.doi.org/10.1007/s40295-016-0085-1.
[70] S.N. Adeli, V.J. Lappas, B. Wie, A scalable bus-based attitude control system for Solar Sails, Adv. Space Res. 48 (11) (2011) 1836–1847.
[71] B. Wie, D. Murphy, Solar-sail attitude control design for a flight validation mission, J. Spacecr. Rocket. 44 (2007) 809–821.
[72] C. Scholz, D. Romagnoli, B. Dachwald, S. Theil, Performance analysis of an attitude control system for solar sails using sliding masses, Adv. Space Res. 48 (2011) 1822–1835.
[73] B. Fu, G. Gede, F. Eke, Controllability of a square solar sail with movable membrane tips, Proc. Inst. Mech. Eng. Part G—J. Aerosp. Eng., 2016, in press.
[74] B. Fu, F. Eke, Further investigation of the body torques on a square solar sail due to the displacement of the sail attachment points, Aerosp. Sci. Technol. 50 (2016) 281–294.
[75] R.S. Blomquist, Heliogyro control (Ph.D.), Carnegie Mellon University, 2009.
[76] W. Wilkie, J. Warren, L. Horta, K. Lyle, J.-n. Juang, C.S. Gibbs, E.H. Dowell, D. Guerrant, D. Lawrence, Recent advances in heliogyro solar sail structural dynamics, stability, and control research (AIAA 2015-0431), in: AIAA SciTech, 2015. http://dx.doi.org/10.2514/6.2015-0431.
[77] D. Guerrant, D. Lawrence, Tactics for heliogyro solar sail attitude control via blade pitching, J. Guid. Control Dyn. 38 (9) (2015) 1785–1799.
[78] J.C. Van Der Ha, V.J. Lappas, Long-term attitude drift of a spinning spacecraft under solar radiation torques, J. Guid. Control Dyn. 30 (5) (2007) 1470–1479.
[79] R. McKay, M. Macdonald, J. Biggs, C. McInnes, Survey of highly non-Keplerian orbits with low-thrust propulsion, J. Guid. Control Dyn. 34 (3) (2011) 645–666.
[80] C.R. McInnes, A.J.C. McDonald, J.F.L. Simmons, E.W. MacDonald, Solar sail parking in restricted 3-body systems, J. Guid. Control Dyn. 17 (1994) 399–406.
[81] A. Farrés, A. Jorba, Periodic and quasi-periodic motions of a solar sail close to SL1 in the Earth–Sun system, Celest. Mech. Dyn. Astron. 107 (1–2) (2010) 233–253.
[82] P. Verrier, T. Waters, J. Sieber, Evolution of the L1 halo family in the radial solar sail circular restricted three-body problem, Celest. Mech. Dyn. Astron. 120 (4) (2014) 373–400.
[83] T.J. Waters, C.R. McInnes, Solar sail dynamics in the three-body problem: homoclinic paths of points and orbits, Int. J. Non-Linear Mech. 43 (6) (2008) 490–496.
[84] H. Baoyin, C.R. McInnes, Solar sail equilibria in the elliptical restricted three-body problem, J. Guid. Control Dyn. 29 (3) (2006) 538–543.
[85] G. Aliasi, G. Mengali, A.A. Quarta, Artificial equilibrium points for a generalized sail in the elliptic restricted three-body problem, Celest. Mech. Dyn. Astron. 114 (2012) 181–200.
[86] T.J. Waters, C.R. McInnes, Invariant manifolds and orbit control in the solar sail three-body problem, J. Guid. Control Dyn. 31 (3) (2008) 554–562.
[87] R.L. Forward, Statite—a spacecraft that does not orbit, J. Spacecr. Rocket. 28 (5) (1991) 606–611.
[88] M. Macdonald, Solar sailing: applications and technology advancement, in: T. Smiljanic (Ed.), Advances in Spacecraft Technologies, vol. 1901, InTech, Rijeka, Croatia, 2011, pp. 35–60 (Chapter 2).
[89] A. Pukniel, The dynamics and control of the cubesail mission—a solar sailing demonstration (Ph.D. dissertation), University of Illinois at Urbana-Champaign, 2010.
[90] M.T. Nehrenz, Initial Design and Simulation of the Attitude Determination and Control System for LightSail-1, Senior Project, California Polytechnic State University, San Luis Obispo, 2010.
[91] L. Johnson, M. Whorton, A. Heaton, R. Pinson, G. Laue, C. Adams, NanoSail-D: a solar sail demonstration mission, Acta Astronaut. 68 (5–6) (2011) 571–575.
[92] L. Johnson, R. Young, E. Montgomery, D. Alhorn, Status of solar sail technology within NASA, Adv. Space Res. 48 (2011) 1687–1694.
[93] M. Macdonald, C. McInnes, D. Alexander, A. Sandman, GeoSail: exploring the magnetosphere using a low-cost solar sail, Acta Astronaut. 59 (2006) 757–767.
[94] M. Macdonald, G.W. Hughes, C.R. McInnes, A. Lyngvi, P. Falkner, A. Atzei, Solar polar orbiter: a solar sail technology reference study, J. Spacecr. Rocket. 43 (5) (2006) 960–972.
[95] T. Appourchaux, P. Liewer, M. Watt, D. Alexander, V. Andretta, F. Auchère, P. D'Arrigo, J. Ayon, T. Corbard, S. Fineschi, W. Finsterle, L. Floyd, G. Garbe, L. Gizon, D. Hassler, L. Harra, A. Kosovichev, J. Leibacher, M. Leipold, N. Murphy, M. Maksimovic, V. Martinez-Pillet, B.S.A. Matthews, R. Mewaldt, D. Moses, J. Newmark, S. Régnier, W. Schmutz, D. Socker, D. Spadaro, M. Stuttard, C. Trosseille, R. Ulrich, M. Velli, A. Vourlidas, C.R. Wimmer-Schweingruber, T. Zurbuchen, POLAR investigation of the Sun—POLARIS, Exp. Astron. 23 (2009) 1079–1117.
[96] A. Lyngvi, P. Falkner, A. Peacock, The interstellar heliopause probe technology reference study, Adv. Space Res. 35 (2005) 2073–2077.
[97] N. Barnes, W. Derbes, C. Player, B. Diedrich, Sunjammer: a solar sail demonstration, in: Advances in Solar Sailing, vol. 1, 2014, pp. 115–126.
[98] J. Fernandez, G. Prassinos, V. Lappas, S. Erb, Deployment mechanisms of a gossamer satellite deorbiter, in: 2013 15th European Space Mechanisms and Tribology Symposium, 2013.
[99] M. Macdonald, G.W. Hughes, C. McInnes, A. Lyngvi, P. Falkner, A. Atzei, GeoSail: an elegant solar sail demonstration mission, J. Spacecr. Rocket. 44 (4) (2007) 784–796.
[100] M.E. Leopold, O. Wagner, Mercury sun-synchronous polar orbits using solar sail propulsion, J. Guid. Control Dyn. 19 (6) (1996) 1337–1341.
[101] G.L. Matloff, T. Taylor, C. Powell, T. Moton, Phobos/deimos sample return via solar sail, Ann. N. Y. Acad. Sci. 1065 (2005) 429–440.
[102] G.W. Hughes, M. Macdonald, C.R. Mcinnes, A. Atzei, P. Falkner, Sample return from Mercury and other terrestrial planets using solar sail propulsion, J. Spacecr. Rocket. 43 (4) (2006) 828–835.
[103] G.W. Hughes, M. Macdonald, C.R. McInnes, A. Atzei, P. Falkner, Terrestrial planet sample return missions using solar sail propulsion, Acta Astronaut. 59 (2006) 797–806.
[104] B. Wie, Thrust vector control analysis and design for solar-sail spacecraft, J. Spacecr. Rocket. 44 (3) (2007) 545–557.
[105] B. Wie, Hovering control of a solar sail gravity tractor spacecraft for asteroid deflection, in: Advances in the Astronautical Sciences, vol. 127, 2007, pp. 673–696.
[106] B. Wie, Dynamics and control of gravity tractor spacecraft for asteroid deflection, J. Guid. Control Dyn. 31 (5) (2008) 1413–1423.
[107] S. Gong, J. Li, B. Hexi, Formation flying solar-sail gravity tractors in displaced orbit for towing near-Earth asteroids, Celest. Mech. Dyn. Astron. 105 (1) (2009) 159–177.
[108] M.J. Sonter, The technical and economic feasibility of mining the near-earth asteroids, Acta Astronaut. 41 (1997) 637–647.
[109] S.D. Ross, Near-Earth Asteroid Mining (Caltech 107-81), Technical Report, Caltech Internal Report, 2001.

Please cite this article as: B. Fu, et al., Solar sail technology—A state of the art review, Progress in Aerospace Sciences (2016), http://dx.doi.org/10.1016/j.paerosci.2016.07.001

[110] M. Macdonald, Advances in Solar Sailing, Springer Praxis, Chichester, UK, 2014.
[111] J.M. Fernandez, L. Visagie, M. Schenk, O.R. Stohlman, G.S. Aglietti, V.J. Lappas, S. Erb, Design and development of a Gossamer sail system for deorbiting in low earth orbit, Acta Astronaut. 103 (2014) 204–225.
[112] M. Macdonald, C.R. McInnes, C. Bewick, L. Visagie, V. Lappas, S. Erb, Concept-of-operations disposal analysis of spacecraft by gossamer structure, J. Spacecr. Rocket. 52 (2) (2015) 517–525.
[113] C. Lucking, C. Colombo, C.R. Mcinnes, Solar radiation pressure-augmented deorbiting: passive end-of-life disposal from high-altitude orbits, J. Spacecr. Rocket. 50 (6) (2013) 1256–1267.
[114] M. Macdonald, C. McInnes, G. Hughes, Technology requirements of exploration beyond Neptune by solar sail propulsion, J. Spacecr. Rocket. 47 (3) (2010) 472–483.
[115] G.L. Matloff, The beryllium hollow-body solar sail and interstellar travel, JBIS – J. Br. Interplanet. Soc. 59 (2006) 349–354.
[116] B. Dachwald, M. Macdonald, C.R. McInnes, G. Mengali, A.A. Quarta, Impact of optical degradation on solar sail mission performance, J. Spacecr. Rocket. 44 (4) (2007) 740–749.
[117] B. Woo, K.M. Ertmer, V.L. Coverstone, R.L. Burton, G.F. Benavides, D.L. Carroll, Deployment experiment for ultralarge solar sail system (ultrasail), J. Spacecr. Rocket. 48 (2011) 874–880.
[118] V. Mayorova, A. Popov, N. Nerovnyy, D. Rachkin, S. Tenenbaum, ISS-based solar sail deployment experiment "BMSTU- Sail", in: M. Macdonald (Ed.), Advances in Solar Sailing, Springer Praxis, Chichester, UK, 2014 (Chapter I).
[119] W. Keats Wilkie, Heliogyro solar sail research at NASA, in: M. Macdonald (Ed.), Advances in Solar Sailing, Springer Praxis, Chichester, UK, 2014, pp. 631–650 (Chapter IV).
[120] M. Leipold, C.E. Garner, R. Freeland, A. Hermann, M. Noca, G. Pagel, W. Seboldt, G. Sprague, ODISSEE—a proposal for demonstration of a solar sail in earth orbit, Acta Astronaut. 45 (4) (1999) 557–566.
[121] D.S.A. De Focatiis, S.D. Guest, Deployable membranes designed from folding tree leaves, Philos. Trans. Ser. A: Math. Phys. Eng. Sci. 360 (1791) (2002) 227–238.
[122] F. Dalla Vedova, H. Henrion, M. Leipold, T. Girot, R. Vaudemont, T. Belmonte, K. Fleury, O. Le Couls, The Solar Sail Materials (SSM) project—status of activities, Adv. Space Res. 48 (2011) 1922–1926.
[123] V. Lappas, N. Adeli, L. Visagie, J. Fernandez, T. Theodorou, W. Steyn, M. Perren, CubeSail: a low cost CubeSat based solar sail demonstration mission, Adv. Space Res. 48 (11) (2011) 1890–1901.
[124] A. Papa, S. Pellegrino, Systematically creased thin-film membrane structures, J. Spacecr. Rocket. 45 (1) (2008) 10–18.
[125] J.A. Banik, T.W. Murphey, Synchronous deployed solar sail subsystem design concept, in: 48th AIAA/ASME/ASCE/AHS/ASC Structures, Structural Dynamics, and Materials Conference, AIAA, Honolulu, US, 2007.
[126] J.A. Banik, T.W. Murphey, H.-P. Dumm, Synchronous deployed solar sail concept demonstration, in: 49th AIAA/ASME/ASCE/AHS/ASC Structures, Structural Dynamics, and Materials Conference, AIAA, Schaumburg, US, 2008.
[127] M. Salama, C. White, R. Leland, Ground demonstration of a spinning solar sail deployment concept, J. Spacecr. Rocket. 40 (2003) 9–14.
[128] N. Okuizumi, T. Yamamoto, Centrifugal deployment of membrane with spiral folding: experiment and simulation, J. Space Eng. 2 (1) (2009) 41–50.
[129] J.M. Fernandez, V.J. Lappas, A.J. Daton-Lovett, Completely stripped solar sail concept using bi-stable reeled composite booms, Acta Astronaut. 69 (2011) 78–85.
[130] C. Sickinger, L. Herbeck, E. Breitbach, Structural engineering on deployable CFRP booms for a solar propelled sailcraft, Acta Astronaut. 58 (2006) 185–196.
[131] J. Block, M. Straubel, M. Wiedemann, Ultralight deployable booms for solar sails and other large gossamer structures in space, Acta Astronaut. 68 (2011) 984–992.
[132] G. Greschik, Solar sail scalability and a "truly scalable" architecture: the space tow, J. Spacecr. Rocket. 44 (2007) 831–839.
[133] M.A. Brown, A deployable mast for solar sails in the range of 100–1000 m, Adv. Space Res. 48 (2011) 1747–1753.
[134] V. Lappas, B. Wie, C.R. McInnes, L. Tarabini, L. Gomes, K. Wallace, Microsolar sails for Earth magnetotail monitoring, J. Spacecr. Rocket. 44 (4) (2007) 840–848.
[135] B. Cassenti, G.L. Matloff, J. Strobl, The structural response and stability of interstellar solar sails, J. Br. Interplanet. Soc. 49 (9) (1996) 345–350.
[136] I. Stanciulescu, L.N. Virgin, T.A. Laursen, Slender solar sail booms: finite element analysis, J. Spacecr. Rocket. 44 (2007) 528–537.
[137] G. Genta, E. Brusa, C. Delprete, Second approximation structural assessment of the Aurora solar sail spacecraft, Acta Astronaut. 54 (2004) 115–125.
[138] J. Liu, N. Cui, F. Shen, S. Rong, Dynamics of highly-flexible solar sail subjected to various forces, Acta Astronaut. 103 (2014) 55–72.
[139] J.L. Gaspar, T.W. Jones, D.M. Murphy, Solar sail structural characterization test program, J. Spacecr. Rocket. 44 (2007) 765–783.
[140] C.S. Gibbs, E.H. Dowell, Membrane paradox for solar sails, AIAA J. 52 (12) (2014) 2904–2906.
[141] Y.W. Wong, S. Pellegrino, Prediction of wrinkle amplitudes in square solar sails, in: 44th AIAA/ASME/ASCE/AHS/ASC Structures, Structural Dynamics, and Material Conference, Norfold, VA, http://dx.doi.org/10.2514/6.2003-1982, 2003.
[142] Y.W. Wong, S. Pellegrino, Wrinkled membranes part II: analytical models, J. Mater. Struct. 1 (1) (2006) 27–61.
[143] Y.W. Wong, S. Pellegrino, Wrinkled membranes part I: experiments, J. Mater. Struct. 1 (1) (2006) 3–25.
[144] R.Y.A. Kezerashvili, Solar sail interstellar travel: 1. Thickness of solar sail films, JBIS - J. Br. Interplanet. Soc. 61 (2008) 430–439.
[145] R.Y. Kezerashvili, Thickness requirement for solar sail foils, Acta Astronaut. 65 (2009) 507–518.
[146] G. Mengali, A.A. Quarta, Tradeoff performance of hybrid low-thrust propulsion system, J. Spacecr. Rocket. 44 (6) (2007) 1263–1270.
[147] M. Ceriotti, C.R. McInnes, Hybrid solar sail and solar electric propulsion for novel Earth observation missions, Acta Astronaut. 69 (2011) 809–821.
[148] G. Wawrzyniak, The dynamics and control of solar-sail spacecraft in displaced lunar orbits (Ph.D. thesis), Purdue University, 2011.

Please cite this article as: B. Fu, et al., Solar sail technology—A state of the art review, Progress in Aerospace Sciences (2016), http://dx.doi.org/10.1016/j.paerosci.2016.07.001